Received: 21 December 2023 | Revised: 14 February 2024 | Accepted: 2 April 2024

DOI: 10.1002/dro2.131

REVIEW ARTICLE

Droplet WILEY

Icephobic materials and strategies: From bio-inspirations to smart systems

Xinlin Li[1] | **Yan Liu**[2,3] | **Zhichun Zhang**[1] | **Yanju Liu**[4] | **Jinsong Leng**[1]

[1]Centre for Composite Materials and Structures, School of Astronautics, Harbin Institute of Technology, Harbin, China

[2]Key Laboratory of Bionic Engineering (Ministry of Education), College of Biological and Agricultural Engineering, Jilin University, Changchun, China

[3]Institute of Structured and Architected Materials, Liaoning Academy of Materials, Shenyang, China

[4]Department of Astronautical Science and Mechanics, Harbin Institute of Technology, Harbin, China

Correspondence
Yan Liu, Key Laboratory of Bionic Engineering (Ministry of Education), College of Biological and Agricultural Engineering, Jilin University, Changchun 130022, China.
Email: lyyw@jlu.edu.cn

Yanju Liu, Department of Astronautical Science and Mechanics, Harbin Institute of Technology, Harbin 150080, China.
Email: yj_liu@hit.edu.cn

Funding information
National Natural Science Foundation of China, Grant/Award Number: 12102105; China Postdoctoral Science Foundation, Grant/Award Number: 2021M690834; Postdoctoral Science Foundation of Heilongjiang Province, Grant/Award Number: LBH-Z21156; Foundation for Innovative Research Groups of the National Natural Science Foundation of China, Grant/Award Number: 52021003

Abstract

Unwanted ice formations may cause severe functional degradations of facilities and also have a negative impact on their lifespans. Avoiding and removing ice accumulation is always a hot topic in the industrial and technological field. Bionic functional surfaces have been greatly studied for several decades and have proved to be excellent candidates for passive anti-/deicing applications. However, the drawbacks limit their potential industrial uses under harsh conditions, like low temperatures and high humidity. Most researches on bionic surfaces are focused on a certain function of natural creatures and their underlined fundamental theories are revealed by taking the interface as the static. Actually, living organisms, either plants or animals, are often sensitive and responsive to their surroundings, avoiding risks and even self-repairing upon damage. From this prospect, a novel view of the bionic icephobic materials has been proposed in the present review, which is expected to be studied and designed by taking the biological species as a system. As two representative icephobic materials, the anti-/deicing theories of superhydrophobic and slippery surfaces are first discussed. Further, the recent progress of smart icephobic strategies is summarized from interfaces to substrates. We aim to provide new bionic insights on designing future icephobic strategies.

INTRODUCTION

Ice accumulation on infrastructures and facilities has caused tremendous damage to industrial processes and individual life,[1,2] such as in aircraft,[3] high-speed trains,[4] solar panels,[5] and so on. For example, the bogies of highspeed trains are easily covered by snow and ice in middle-high latitude regions in winter. For instance, the snow/ice accumulation significantly restrains the displacements of springs, which results in intensive vibrations and safety risks.[6] Researchers have made great efforts to overcome these problems by making facilities free from ice. When considering the operation conditions of relative humidity (RH), surface/environmental temperature, and impact

velocity, the ice formations on solid surfaces generally include frost, mixed ice, and glaze ice.[7] To remove the ice from the solid surfaces, the most conventional methods include vapor heating,[8] hot water treatment,[9] electro-thermal melting,[10] mechanical vibration,[11] and use of chemicals.[12] However, the drawbacks of the high energy costs and environmental pollution limit the use of these methods as deicing strategies.[13–15]

Water droplets that are frozen on solid surfaces are generally involved in adsorption, nucleation, and icing processes. Ice-free surfaces will be easily obtained if any of these processes can be diminished.[16,17] Therefore, an effective way to hinder ice formation is to design a novel material that facilitates the anti-icing and deicing processes.[18–21] Passive anti-/deicing methods have recently gained large attention and are identified as promising approaches toward ice prevention.[22,23] Also, there are novel ideas for the design of icephobic materials that are based on natural organisms, with their unique nonwetting characteristics.[24,25] Inspired by the lotus leaves, superhydrophobic material surfaces show good self-cleaning properties, with water contact angles larger than 150° and water sliding angles smaller than 10°. On these surfaces, the water droplets are suspended over the micro/nanostructures by an air cushion.[26–28] The interface, composed of a complex and intermittent solid–liquid–air tri-phase (called the Cassie state), is dominated by a rough surface structure and low surface energy.[29,30] The superhydrophobic surfaces (SHSs) are widely considered as ideal icephobic candidates, which is due to their excellent water repulsion capabilities and ice adhesion reduction properties.[31,32] However, the SHSs have been reported to be ineffective under extreme conditions. They are also subject to damage due to their fragile micro/nanostructures, which limits their potential icephobicities.[33–35] Consequently, the modifications of the physical or chemical properties of superhydrophobic materials have become very popular in recent decades.

Another icephobic material that has been widely popular is the liquid-infused surface (LIS), which mimics the unique slippery character of the "pitcher" of Nepenthes.[36,37] In contrast to the SHS, the LIS presents a solid–liquid–liquid tri-phase system. On this surface, the air within the hierarchical or porous material has been replaced by the infusion of a slippery liquid phase.[38] Therefore, the water droplets cannot adhere to the gaps of the surface morphologies, which is the reason for the improved icephobicity of the LIS (as compared with the SHS) in a high humidity environment.[39,40] It should be noted that the anti-icing hydrogel material is also a liquid-layer type of material. By controlling the structures and dynamics of the interfacial water-like antifreeze proteins, it shows an ice nucleation inhibition property even at temperatures lower than −30°C.[41] The lubricants can also be the phase change materials, which are commonly incorporated into polymeric matrices. Their icephobic properties are recognized as a release or absorption of latent heat. These icephobic properties are also recognized as a volume change, which involves a combination of air type and liquid type.[42] Therefore, an effective icephobicity requires a surface/gas interface or surface/liquid interface, to reduce the water/ice adhesion on the solid surface. The liquid must then be immiscible with water.

Water/ice layers, interfaces, and substrates are all important for the icing process of water. By considering the different physical properties of water/ice, it is a good strategy to provide the interfaces and substrates with smart performances. Smart interfaces and substrates that show dynamic water prevention, ice nucleation inhibition, ice adhesion reduction, and stimuli-responsive ice removal can achieve improved anti-icing properties even in harsh environments (Figure 1). For the smart interfaces, the water/ice adhesion can be modified based on the physical/chemical properties of the liquid and air within the micro/nanostructures. Furthermore, the smart substrates can detach the water/ice in response to external stimuli. Moreover, natural organisms do not generally display a certain type of function, but instead a system of functions. Inspired by this system of functions, smart icephobic systems have for the first time (to the best of the authors knowledge) been proposed in the present review, with which it is possible to design a novel anti-/deicing strategy. Biomimetic icephobic materials of air-layer type (i.e., solid/gas interfaces) and liquid-layer type (i.e., solid/liquid interfaces) have then been separately discussed, followed by analyses of the corresponding icephobic mechanisms. Furthermore, the current progress of hybrid methods has been introduced, including emerging strategies in combination with passive, or active, methods. Finally, an outlook for the development and applications of bioinspired smart systems has been presented, with the purpose of aiding in the future development of novel icephobic strategies.

BIOINSPIRED ICEPHOBIC MATERIALS

Bio-inspirations from plants and animals

After many years of evolution, biological species (like cuticles of plants and shells of insects) have successfully built specific layers to protect themselves from destruction by the surrounding. Wetting phenomena are generally observed on the skin of animals, which is of large importance to study. It has been revealed that the micro/nanoscale surface topographies and adhered chemicals contribute to the special wetting performances of plants and animals.[47–49]

For plants and animals with an isotropic wettability, the water droplets can easily roll off in any direction on the surface. As illustrated in Figure 2a, the impacting water droplet can completely rebound from the surface, with a reduction in the water–solid contact time. The most representative plant is the lotus leaf with a periodic mastoid microstructure.[57] The lotus seed pod surface exhibits a superhydrophobic self-cleaning property, with a water contact angle of 153.9° ± 2.7° (Figure 2b).[50] For the situation with penguins (Spheniscus humboldti),[51] their nonwetted feathers help to maintain a normal flight status when they are going into water. The feathers are composed of so-called "quasi-hierarchical" structures, and the main shaft (rachis) is covered by numerous barbs (ramus) and barbules[51] (Figure 2c). Like the lotus leaf, water/ice can, thereby, be easily removed from the isotropically wetted surfaces of the feathers, and in any direction on the surfaces. In contrast to isotropic wettability, anisotropic wettability is the situation when water droplets present different rolling behaviors

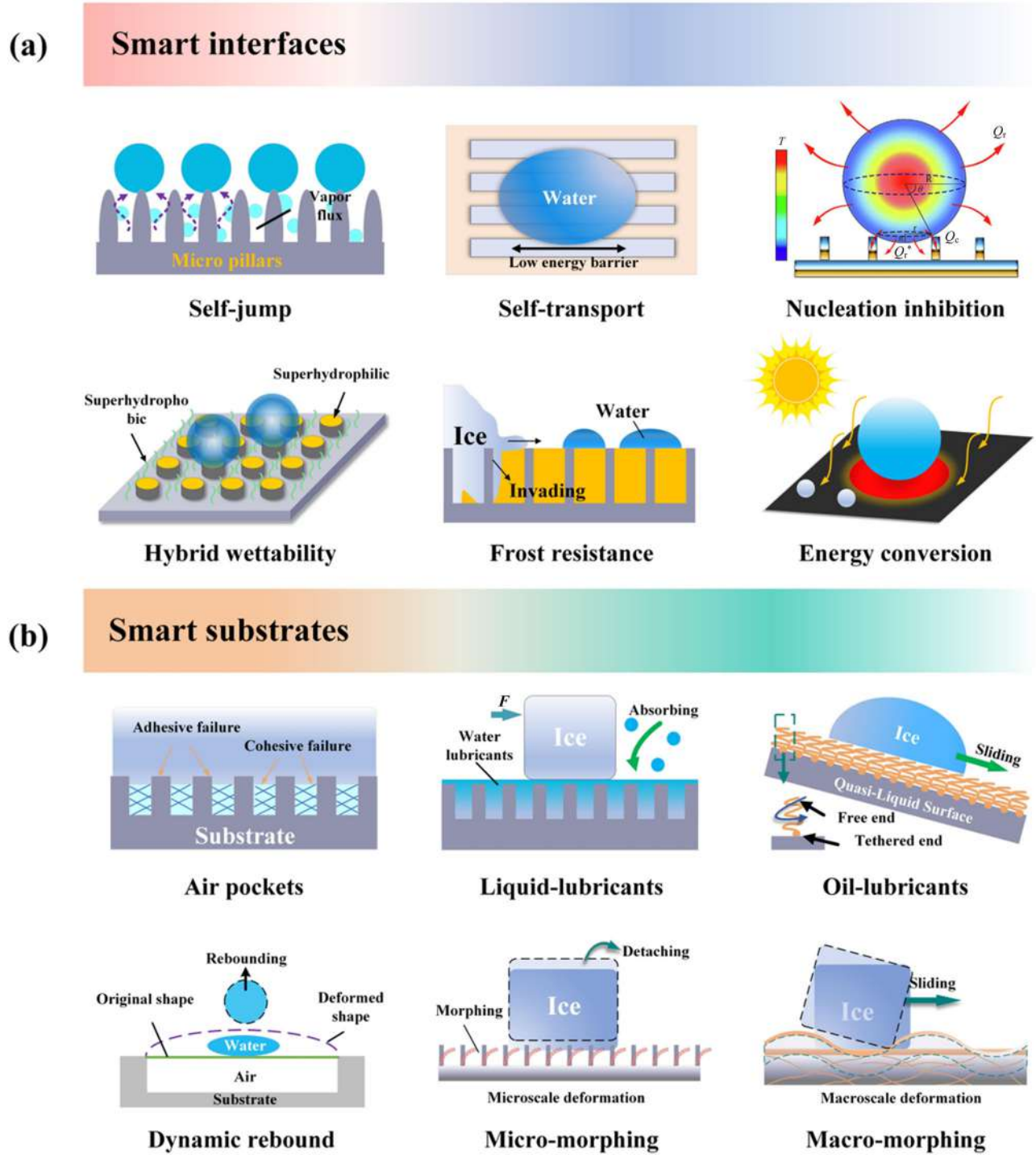

FIGURE 1 Schematics of a smart icephobic system. (a) The smart interfaces can efficiently prevent water/ice adhesion, and (b) the smart substrates can effectively remove ice or melt the ice at the interface. Reproduced with permission.[43–46] Copyright 2020, Elsevier. Copyright 2021, American Chemical Society. Copyright 2020, American Chemical Society. Copyright 2012, AIP Publishing.

in different directions on the surface. As a typical anisotropically wetted surface, water droplets on the rice leaf are more likely to roll off in a direction parallel with the leaf edge (with rolling angles in the range of 3°–5°), rather than in a direction perpendicular to the leaf edge (with rolling angles in the range of 9°–15°). The reason for this behavior is that the microstructure is aligned along the direction of the leaf edge.[59] In contrast, the hybrid wettability of a surface involves two, or more, wetting performances simultaneously. The tiny droplets with sizes on the microscale prefer to coalesce with adjacent larger droplets and are, thereby, removed without adhering to the surface (Figure 2d). Salvinia molesta[52,60] has a unique eggbeater-shaped microstructure, which is generally covered with wax nanocrystals. The exception is

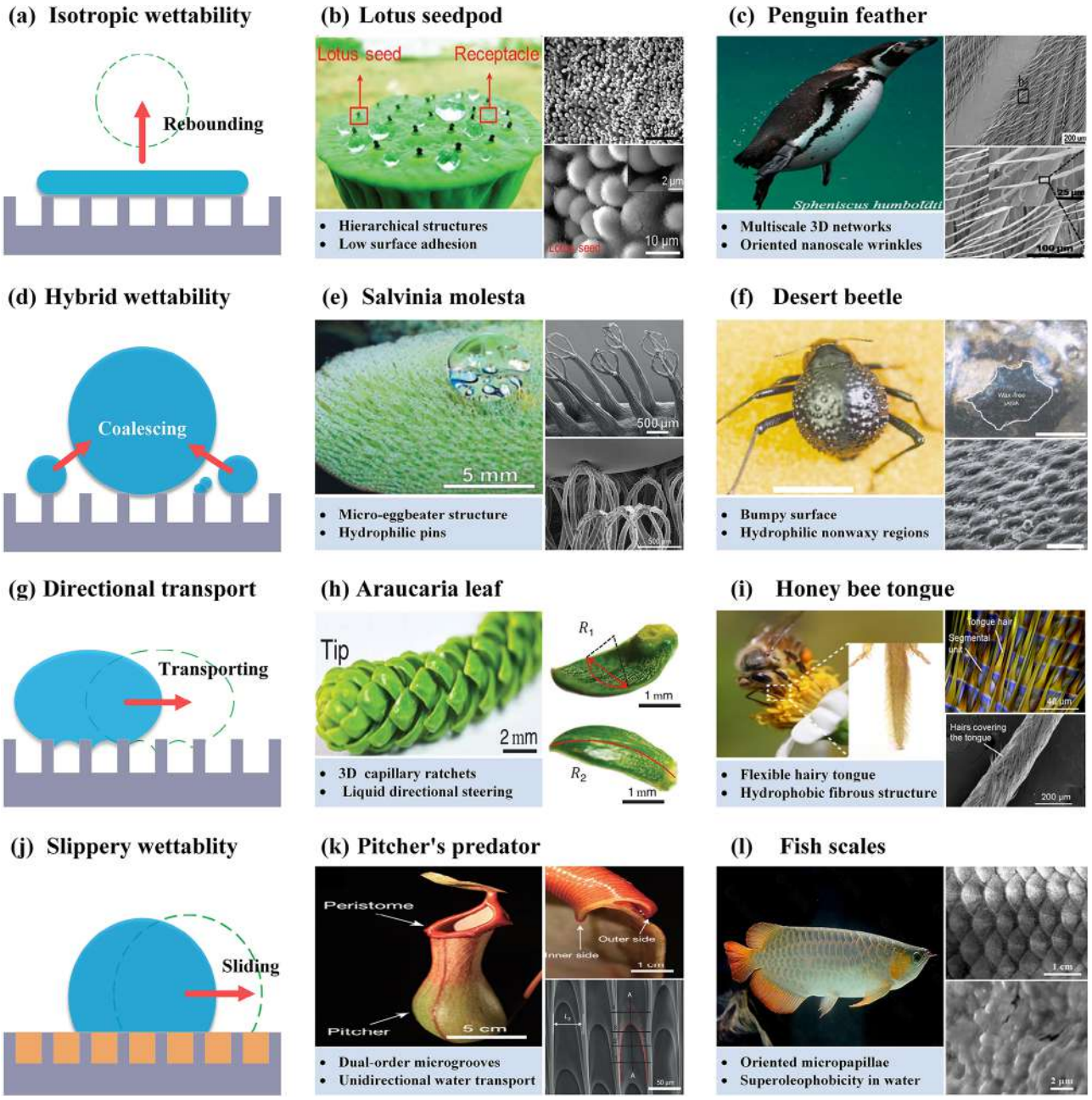

FIGURE 2 Representative plants and animals with nonwetting surface properties. (a) Schematics of water dynamics on isotropic superhydrophobic surfaces, with representative examples: (b) lotus seedpod. Reproduced with permission.[50] Copyright 2017, Wiley-VCH. (c) Penguin feather. Reproduced with permission.[51] Copyright 2016, American Chemical Society. (d) Schematics of water dynamics on hybrid wetting surfaces, with representative examples: (e) Salvinia molesta. Reproduced with permission.[52] Copyright 2010, Wiley-VCH. (f) Desert beetle. Reproduced with permission.[53] Copyright 2001, Springer Nature. (g) Schematics of water dynamics on directional transporting surfaces, with representative samples: (h) Araucaria leaf. Reproduced with permission.[54] Copyright 2021, The American Association for the Advancement of Science. (i) Honey bee tongue. Reproduced with permission.[55] Copyright 2022, American Chemical Society. (j) Schematics of water dynamics on slippery surfaces, with representative examples: (k) predator pitcher. Reproduced with permission.[36] Copyright 2016, Springer Nature. (l) Fish scales. Reproduced with permission.[56] Copyright 2009, Wiley-VCH.

the top areas with dead cells (Figure 2e). These hydrophilic areas can easily catch the smaller water droplets, but larger droplets will roll off when tilting, or vibrating, the surface. Moreover, the incorporation of hydrophilic areas and other hydrophobic hairs can stabilize the air–water interface against pressure fluctuations. Furthermore, different from its nonsticking mechanism, the beetles in the Namib Desert[53] have created unique bumpy surfaces for water collection, with the aim to survive in this dry environment. The nonuniform distribution of wax-coated (hydrophobic) and nonwaxy regions (hydrophilic) can effectively condensate the water vapor for drinking (Figure 2f). This

property is also helpful to increase the removal possibility of the water/ice by forming intermitted water/ice particles.

Moreover, there are many biological surfaces with the characteristics of a directional transport of water droplets. This transport mainly depends on the gradients of the surface energy and the Laplace pressure as the driving forces.[61–63] Thus, the water droplets are self-driven from the surface before being frozen (Figure 2g). One representative plant is the Araucaria leaf, onto which water droplets with different surface tensions can be selectively transported by periodically arranged ratchets[54] (Figure 2h). A similar characteristic has been found on the tongue of the honeybee (Apis mellifera L.).[55] Its flexible tongue is covered with fine structures of hydrophobic hairs, which is helpful for separation and for the reduction of friction caused by the capillary force (Figure 2i). During the liquid capturing process, the capillary force is dominating over the gravity. Under certain conditions, the self-driving performances of these types of surfaces are beneficial for water/ice removal with less energy consumption. Another type of representative surface is the slippery surface, which normally consists of lubricants and microstructures.[64,65] In contrast to the air layer (in a solid/air interface), the lubricant (in a solid/lubricant interface) will not only prevent the intrusion of water droplets, but it will also slide the adhered water/ice (Figure 2j). As being the most popular prototype of slippery surfaces, the "peristome" of the predatory pitcher plant[36] has a two-order hierarchical arrangement of radial ridges, and the vertical gradients drive the directional water transport (Figure 2k). Moreover, fishes can easily swim due to a reduced surface friction, which is attributed to the protective fish-scales and the slippery mucus (Figure 2l).[56] The unique slippery property hinders the water/ice adhesion, which results in an excellent anti-/deicing performance. As discussed above, the wettability and structural parameters of typical animal surfaces are important for the design of potential icephobic materials. These data are summarized and presented in Table S1. Thus, the surface morphology and chemical surface adsorbates are important for the modification of the surface wettability.[66,67]

Consequently, the ideal icephobic strategies that are inspired by nature involve four physical characteristics and one durability property[68]; (I) the adhered water droplets completely rebound from the surface with a short solid–liquid contact time ($t_{contact}$). (II) The heterogeneous ice nucleation is prevented by an ultralong freezing delay time ($t_{freezing}$) and an ultralow icing temperature (T_{icing}). (III) There is a self-removal capability of the condensed water under supersaturated humidity conditions. (IV) There is an ultralow adhesion strength of the ice in the ice–solid interface and (V) high robustness of the surface system. Generally, the characteristics (I)–(III) are regarded as anti-icing processes and (IV) is regarded as a deicing process. Due to the robustness of the icephobic surface, it does not only demonstrate durability against different harsh working conditions, but it also shows self-healing and reproduction abilities.[69] Most importantly, animals and plants are generally the organisms that undergo the most proper reactions with the surroundings for the purpose of survival. Therefore, a novel smart system with superior anti-icing and deicing performances can be constructed by understanding the mechanisms on animal surfaces.

Preparation approaches for icephobic materials

Inspired by natural surfaces, artificial SHSs can be fabricated by top-down approaches, bottom-up approaches, and approaches by combining the two methods (Supporting Information: Figure S1a).[70,71] The details about the fabrication methods are listed in Supporting Information: Table S2. The top-down approach refers to the fabrication process that utilizes high-precision tools to obtain micro/nanostructures from a large piece of material (such as photolithography, etching, and micromachining). The manufacturing processes of nanoimprint lithography (NIL) and templating methods should be recognized as top-down methods since the templates are generally fabricated by specific top-down methods.[72] The bottom-up approach refers to processes where small components are assembled from atoms or molecules. More extensive and organized systems can, thereby, be constructed following the natural physical principles or external driving forces.[72]

As a convenient and efficient approach, coating technologies are favored in providing the substrates with superhydrophobic performances, which is the most promising commercial application.[73–77] Zhu et al.[78] prepared a transparent coating by spraying a mixed dispersion of polydimethylsiloxane (PDMS) and commercial titanium dioxide as a protective layer. A uniform nanoarchitecture of PDMS was, thereafter, deposited on the substrate. As tested by a high-speed water jet and numerous cycles of tape peeling, this coating could maintain a high transmittance and mechanochemical robustness and could be used as an icephobic material on windshields, or mirrors. Tian et al.[79] prepared superhydrophobic Zn–Fe coatings with Echinopsis multiplex-like hierarchical micro/nanostructures on carbon steel plates by using constant potential polarization electrodeposition. The coatings exhibited high water-repellent performances (wetting contact angle of ~166° and wetting sliding angle of ~4°), high impact resistances, and good anticorrosion properties. In addition, additive manufacturing is another effective way to construct complicated architectures with high precision. As can be seen in Supporting Information: Figure S1b, Yang et al.[60] fabricated biomimetic eggbeater structures of Salvinia molesta leaves by using immersed surface accumulation-based 3D printing. The controllable adhesive forces on the artificial surfaces varied from 23 to 55 μN, depending on the number of eggbeater arms. The unique controllable adhesion properties showed the potential for droplet modifications.

Moreover, researchers have provided some interesting and effective ways to create rough surface structures. Tan et al.[80] reported on a 3D-shrinking method by tuning the prestrain of a nonuniform graphene oxide (GO)-coated spherical balloon. They, thereby, achieved a papillae array like a rose petal. As can be seen in Supporting Information:Figure S1c, they coated a thin GO film on an inflated balloon by using a water evaporation-driven assembly process. A 3D GO-micropapillae were then obtained in the deflating process of the balloon, which was caused by the thickness gradient. Li et al.[81] proposed a similar process to create wrinkled morphologies with shape memory polymer (SMP) particles. They, thereby, used the shape fixity and recovery capabilities of these polymer particles. The shape memory polystyrene (PS) microparticles were first pressed into disk-like shapes using NIL at 140°C (Supporting Information: Figure S1d). Once cooled to room

temperature, the shapes were fixed even after releasing the pressure. After being coated with a thin film of gold nanoparticles, the disk-like shape memory PS microparticles were triggered by external stimuli (direct heating or using toluene vapors) to recover the original ball shape. As a result, the thin film of gold nanoparticles was transformed into various wrinkled structures. This is a promising approach to fabricate smart micro/nanotextured SHSs.

Slippery surfaces are usually fabricated by infusing a viscous liquid into precisely textured surfaces.[39,82,83] The liquid repellence of a LIS is characterized by a contact angle hysteresis smaller than 2.5° and a tilt angle smaller than 5°.[84] The fabrication methods of SHSs can be utilized to manufacture the holding medium of the infused liquid. Peppou-Chapman et al.[85] classified the LIS into three categories; one-dimensional (1D), two-dimensional (2D), and three-dimensional (3D) LIS. The 1D LIS refers to the bonding of the lubricant to the substrate on a molecular scale. The 2D LIS is a substrate surface where the lubricant can be trapped within the nano- and microscale topographical structures by capillary actions. Also, the 3D LIS is characterized by a porous 3D molecular network that is filled with the lubricant. Generally, the 2D and 3D LISs have been widely studied for their high capacity to trap and store lubricants. According to the physical properties of these materials, textured substrates can be prepared by additive approaches and/or by removal approaches. As being one essential part of the LIS, the lubricants should be provided with properties of low surface tension (<30 mN m^{-1}), low vapor pressure (<1 Pa), chemical inertness, and appropriate viscosity (<100 cSt).[85] Two main classes of lubricants are perfluoropolyethers (Krytox series from Dupont) and linear PDMS (silicone oil). Therefore, the typical fabrication method for slippery surfaces can be divided into three parts: (i) formation of hierarchical/porous structures, (ii) surface functionalization with chemicals, and (iii) infusion with lubricants.[86] Consequently, the lubricant will be held in place by a combination of Van-der-Waals forces and capillary forces.[87,88]

ICEPHOBIC LIQUID–AIR INTERFACE

Superhydrophobic surfaces with liquid–air interfaces are well-known for their excellent water-repellent properties. In fact, this type of surface is regarded as the best candidate for icephobic applications. As discussed above, the anti-icing process refers to the prevention of water condensation and ice nucleation on a surface. Also, the deicing process focuses on the removal of ice with, or without, an external energy input.[89]

Reduction of solid–liquid contact time

The water impact process on a surface involves a complex transfer of mass, momentum, and energy in the solid–liquid interface. The ideal strategy for an outstanding anti-icing property is to minimize the contact process between the water droplet and the substrate, which is characterized by the solid–liquid contact time ($t_{contact}$). Generally, the impacting water droplet on a nonwetted surface will experience the processes of contacting, spreading, contracting, and rebounding. In the spreading stage, the water droplets will become extended to the maximum diameter (D_{max}), which can be described by Equation 1[90]:

$$(D_{max}/D_0)\,Re^{-1/5} = P^{1/2}/\left(1.24 + P^{1/2}\right) \quad (1)$$

where D_{max} and D_0 are the maximum diameter and original diameter, respectively. Also, P is the impact parameter ($P = WeRe^{-4/5}$), where We and Re are the Weber number and Reynolds number, respectively. A larger value of We corresponds to a larger deformation of the water droplet (Figure 3a). After the spreading stage, the stored potential energy in the droplet will be transferred into kinetic energy, which results in a complete lift-off of the water droplet.[91] However, the droplet will compress and penetrate into the trapped air in the surface structure with an increased We value, which leads to a transition from a completely rebound state to a sticky state.[92] Furthermore, Richard et al.[102] revealed that the solid–liquid contact time is independent of the impact velocity in the range of 20–230 cm s^{-1}. It is also proportional to the water droplet radius in the range of 0.1–4.0 mm. At high We values, penetration into the substrate surface also takes place during the water impacting process.[91] For a supercooled water droplet and a low We value, the water droplet shows a similar maximum spreading diameter as the room temperature droplet. However, it shows a smaller maximum spreading diameter at a high We value.[103]

Other factors should also be considered when analyzing the dynamic behavior of water droplets in real situations (such as surface inclination,[104] RH,[95] ambient/substrate temperature,[105,106] etc.). For the inclined SHS, the impacting water droplets asymmetrically spread along the lateral and longitudinal directions, which leads to uneven distributions of the front and rear lamella (Figure 3b). In addition, a water rim is formed during the spreading process under the influence of wettability and surface tension forces.[93] Also, the spreading diameter and rebound height of the water droplets decrease with an increase in the inclined surface angle, and the water contact time shows the same trend.[94] Furthermore, with an increase in the ambient humidity, the rebound performances of the water droplets are largely prohibited, which is due to increased surface adhesion. As can be seen in Figure 3c, the rebound heights of the water droplets dramatically decrease when the RH is larger than 95%.[95] At this humidity, the tiny water droplets keep condensing in the micro/nanostructure of the SHS, which leads to a partial, or full, penetration of the air cushion. In addition, the impact of water droplets onto a supercooled surface involves complex physical processes of hydrodynamics, heat transfer, and heterogeneous ice nucleation, which can be expressed by Equation 2.[105]

$$\frac{d^2R}{dt^2} + \left(1 - C\varphi_0 e^{f(T_{interface})} t_c^2\right) R = 0 \quad (2)$$

where R is the dimensionless position of the contact line, C incorporates empirical and theoretical constants, $f(T_{interface})$ is a function of the interface temperature, t_c is the droplet–substrate interface temperature, and φ_0 is the initial features without any ice. The droplets adhere completely onto the SHS at extremely low temperatures. When controlling the impact velocity, directional movements of water droplets

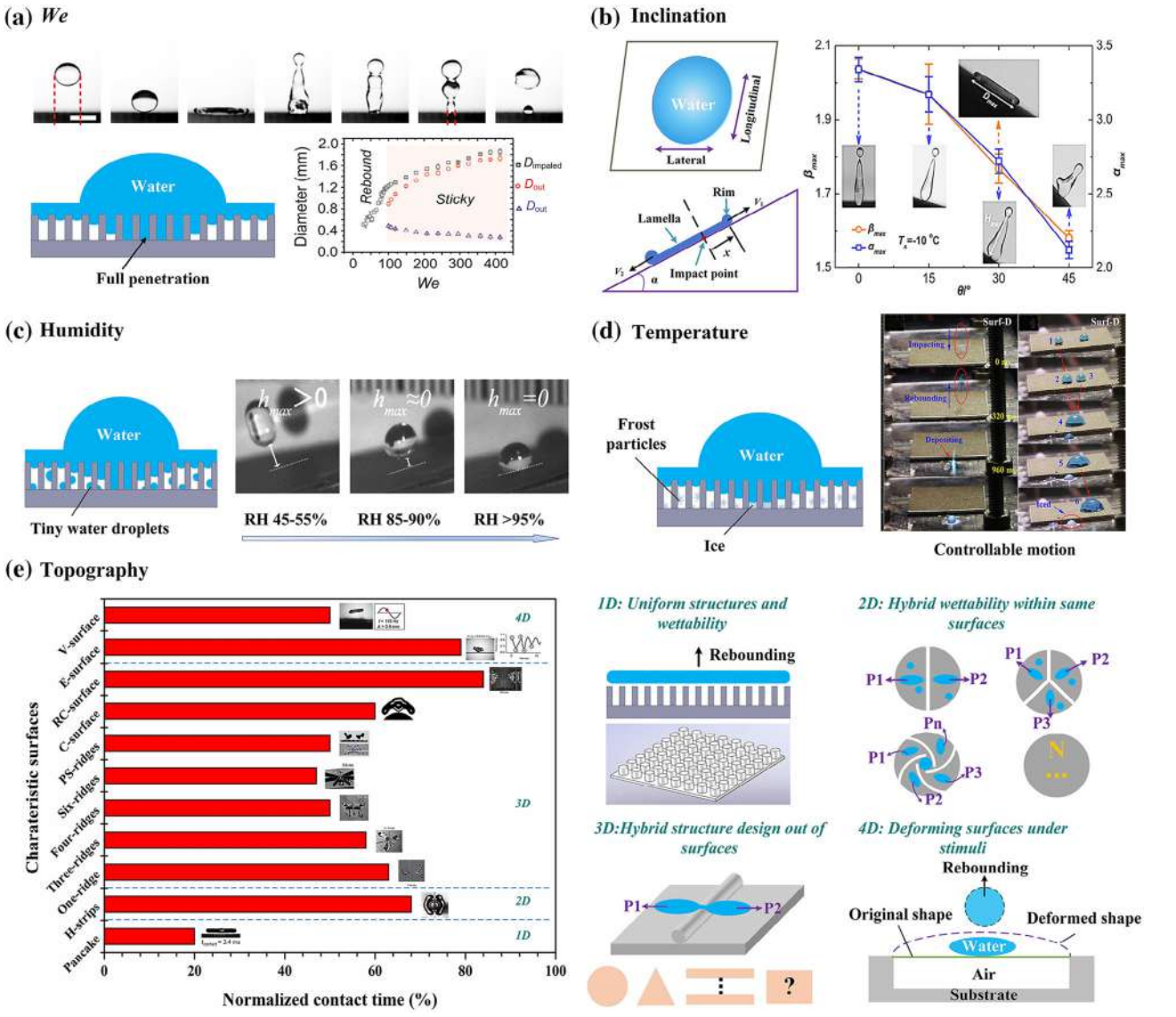

FIGURE 3 Solid–water contact behavior on typical superhydrophobic surfaces. (a) Impact dynamics of water droplets for various *We* values. Reproduced with permission.[91,92] Copyright 2020, National Academy of Sciences. Copyright 2014, American Chemical Society. (b) Impact dynamics of water droplets on inclined surfaces. Reproduced with permission.[93,94] Copyright 2021, American Chemical Society. Copyright 2019, Elsevier. (c) Rebound performances of water droplets at different humidities. Reproduced with permission.[95] Copyright 2013, American Chemical Society. (d) Water droplet dynamics on superhydrophobic surfaces at low temperatures. Reproduced with permission.[43] Copyright 2019, Elsevier. (e) Reduction in contact time for different characteristic surfaces. Reproduced with permission.[30,96–101] Copyright 2015, AIP Publishing. Copyright 2017, American Physical Society. Copyright 2014, Springer Nature. Copyright 2013, Springer Nature. Copyright 2017, Springer Nature. Copyright 2015, Royal Society of Chemistry. Copyright 2015, Springer Nature.

are observed at low temperatures (Figure 3d).[43] This can be attributed to the formation of frost within the surface structure at such low temperatures, which leads to the "Cassie—Wenzel state."[107] The impact center of the water droplets is stuck onto the surface, and the other parts of the droplets keep spreading and "swallow" adjacent droplets. Consequently, the water drop dynamic is dependent on the physical status of the substrate, in addition to the droplet-to-substrate size ratio. Moreover, the impacting performance of the water drops onto the SHS is dependent on the surface energy. The wetting takes place when the surface tension is lower than 56 mN m^{-1}. The wetting pressure and the effective water hammer pressure are then larger than the antiwetting pressure.[108] For aircrafts under Bernoulli and hammer pressures, the increased impact speed leads to a strong adhesion of water/ice onto the SHS.[109]

Regardless of the above-mentioned situations, there are four strategies that have been widely studied for a further reduction of the contact time (Figure 3e). The first strategy is to hinder the impact of water droplets by eliminating the retracting period of the SHS with a uniform structure and wettability. This is identified as the 1D structure. For example, Liu et al.[96] reported on a unique pancake

bouncing behavior on a micro/nanohierarchically textured SHS. The excellent superhydrophobic property enabled the water droplets to detach immediately without experiencing any retractions. In addition, the water contact time was dramatically reduced. It was four times shorter than that of the complete rebound process. If the surface wettability is nonuniform, the hydrodynamics of the impacting water droplets can be modified by creating hydrophilic defects on the SHS. This is identified as the 2D strategy. The water droplets can be split into mini-marbles when impinging onto the hydrophilic regions of the surface at high velocities.[97]

Otherwise, the hydrodynamics of the impacting water droplets can also be altered and the liquid masses can be redistributed by designing hybrid structures outside the surface, which is identified as the 3D strategy. The water droplet contact time is also dramatically affected by the different shapes of the macroscopic superhydrophobic ridges. This is due to the nonaxisymmetric center-assisted recoiling characteristics. Similar to the impacting performances on the Nasturtium plant and Morpho butterfly wings, the water droplets are not immediately split and the time required for recoiling is further decreased.[110] If the number of macroscopic superhydrophobic ridges is increased, the water droplets can be further split into several fragments. From the results proposed by Gauthier et al.,[98] the evaluated contact time is close to $\tau_0/\sqrt{n}$, where τ_0 is the reference contact time on a flat SHS. However, the contact time will not be further reduced by increasing the number of superhydrophobic ridges.[111] For the parallel macroscale superhydrophobic ridges (like on the rice leaf), the water contact time is dependent on the diameters of water droplets and the distances between the macroridges. The contact time can be greatly reduced by 40–50% when the droplet diameter is comparable with the distance between two ridges.[99] For a superhydrophobic cylinder, when the size of the water droplet is comparable with the curvature of a single superhydrophobic ridge, the water droplet exhibits asymmetric bouncing dynamics along two perpendicular directions. This results in a time reduction of 40%.[30] However, the impacting water droplet tends to surround the cylinder, and the separated parts will form a pair of "wings" when the droplet size is larger than the diameter of the superhydrophobic cylinder.[112] Moreover, if the water droplet impacts onto the hierarchical macro/microridges, the water droplet will be detached from the uniquely curved SHS within 4.55 ms.[100]

Alternatively, the surface can be designed to dynamically respond to the impact of the water droplet, which is classified as a 4-dimensional strategy. A flexible SHS can actively disturb this water droplet impact.[113] For instance, Weisensee et al.[101] fabricated superhydrophobic elastic cantilever substrates for this purpose. During the impact of a water droplet to this type of surface, the elastic cantilever substrate transferred the vertical momentum back to the droplet, which is called the springboard effect. Before the retraction was completed, the water droplet lifted off from the surface in an extended 2D shape, which resulted in a contact time that was 21% shorter than that of a rigid SHS. Moreover, Weisensee et al.[101] presented an interesting technique for the study of water droplet impact dynamics. They exerted various vibrating frequencies and amplitudes on the rigid SHSs. As compared with a stationary surface, the contact time of the water droplets could, thereby, be reduced by 50%. In addition, bouncing of the 2D-shaped droplet took place at the critical frequency-dependent impact stage (at an angle of 156°). It is, therefore, essential to maintain the air pockets in the surface structure to minimize the water adhesion possibilities, which can be obtained by controlling the physical status of the superhydrophobic substrates and water droplets. A dramatic decrease in contact time on SHSs is the most critical and influential way to prevent ice coverage.

Freezing delay properties

Water droplets that are sticking onto SHS will freeze to ice at low temperatures. During the icing process, the water droplets undergo ice crystallizations, ice front propagations, and shape changes (Figure 4a). Based on the classical nucleation theory, the icing process on a SHS is commonly recognized as a heterogeneous nucleation process. This type of nucleation process is initiated by impurities and chemical/physical defects in the interface.[114] An ice nucleus will spontaneously form at a nucleation site and lead to an entire phase transition that incorporates additional water molecules (Figure 4b). Generally, the icing process of water droplets on a SHS is characterized by the freezing/icing delay time, which is defined as the time interval from the start of the cooling to the complete freezing. Also, the icing process can be divided into precooling and ice growth stages, where the ice growth stage typically accounts for less than 5% of the total time. The icing process is triggered by the first ice nucleus in a water droplet, and the freezing front quickly moves from the substrate to the top with dramatic shape changes.[117] Factors like droplet size, surface morphology, and cooling rate can significantly affect the freezing delay properties of the water droplets on SHSs. By considering the surface nucleation rate on a modified substrate (J_s) and the water bulk nucleation rate (J_v), the number of generated nucleation sites per second (J_{total}) can be obtained from Equation 3[118,119]:

$$J_{total} = J_s \times S + J_v \times V \tag{3}$$

where S and V are the surface area and bulk volume, respectively. The bulk nucleation can be inhibited by decreasing the V value, which leads to a decrease in total nucleation sites. Consequently, a smaller droplet radius can help to promote a homogeneous nucleation.

Moreover, the hierarchical micro/nanostructures provide the SHSs with the largest freezing delay times, which is due to the smallest solid/liquid contact areas.[120,121] The following methods have been used for the analyses of the freezing delay performances of the surfaces: (i) stabilization of the cooling environment/plate at a specific temperature to record the freezing delay time when the freezing is complete.[122] (ii) Cooling the environment/plate at a specific rate to record the temperature and time when the freezing is complete.[43] By using the latter method, it is possible to establish a relationship between the freezing temperature and the freezing/icing delay time. In addition, it is also possible to calculate the heat loss rate.[123] The heat

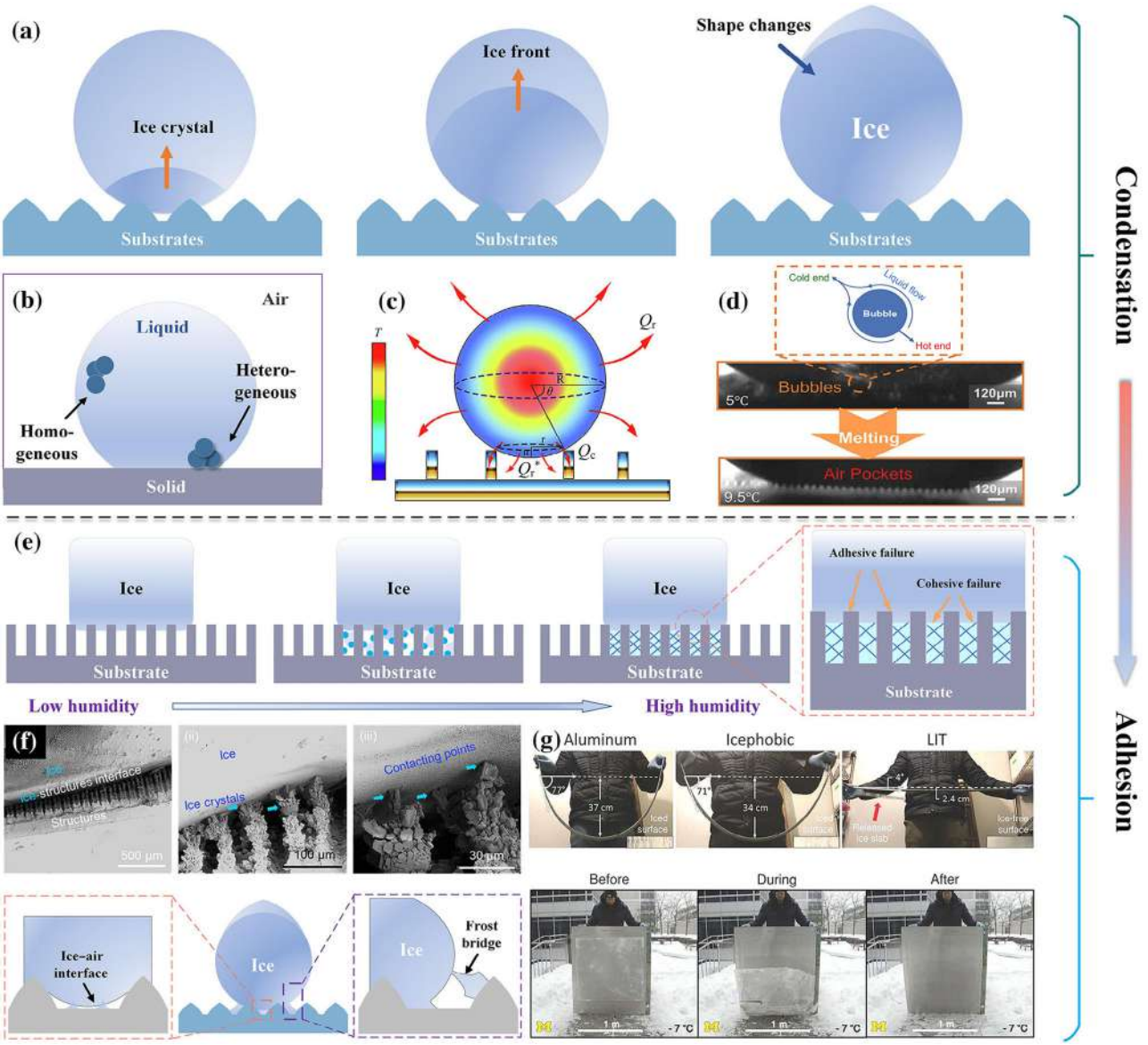

FIGURE 4 Water condensation and adhesion on superhydrophobic surfaces. (a) Schematics of the condensation process. (b) Formations of initial ice nuclei by homogeneous and heterogeneous nucleation. Adapted with permission.[114] Copyright 2015, American Chemical Society. (c) Model of a heat transfer process. Reproduced with permission.[43] Copyright 2019, Elsevier. (d) Melting of a water droplet on a surface with double-scale periodic microcones. Reproduced with permission.[45] Copyright 2022, Springer Nature. (e) Schematics of the humidity-depending ice intrusion.[46] Copyright 2012, AIP Publishing. (f) Cryo-SEM images and schematics of the interfacial contact between ice and a microstructured surface. Reproduced with permission.[115] Copyright 2023, American Chemical Society. (g) Effective large-scale deicing on low-interfacial toughness materials. Reproduced with permission.[116] Copyright 2019, The American Association for the Advancement of Science.

loss of a water droplet on a SHS in a cold environment is illustrated in Figure 4c. These heat losses can be calculated using Equation 4:

$$\Delta Q = Q_c + Q_r + Q_r^* \quad (4)$$

where ΔQ is the total heat loss, Q_c is the heat conduction at the interface, and Q_r and Q_r^* are the convective heat transfer and heat radiation at the liquid–air interface, respectively. However, the heat loss on the hydrophilic surface takes place by only two different pathways, which is due to the complete contact in the solid–liquid interface. Quantitatively, the heat loss rate on the SHS is dramatically reduced compared with the bare surface.[43] Thus, a refined design of the textured surface structure is beneficial for the suppression of the ice nucleation process.[124]

When the freezing is complete, the tiny droplets under high humidity conditions replace the trapped air within the solid structures, leading to the high-adhesion Wenzel state. From the experimental observations of Wang et al.,[45] the contact angle decreases gradually at a reduced surrounding temperature, which can be explained by the icing-induced volume expansion. Interestingly, numerous bubbles are dissolved and frozen in the ice droplets instead of escaping with time (Figure 4d). During the melting process, the tiny bubbles continue to migrate from the nonmelting zone to the melting zone, which is due

to the surface tension gradient. It has been demonstrated that the air pockets that are recovered during the melting process result in a wettability transformation from the Wenzel state to the Cassie-Baxter state. Therefore, the trapped air in the interface can significantly decrease the heat loss of the water droplets and inhibit the ice nucleation process. In addition, the intrusion of water droplets into the gaps of the textured surface structure is fatal for the icephobic performances, resulting in a dramatic acceleration of the freezing process. The vapor droplets continue to condense and are pinned in the microtexture spaces of the surface. Thereafter, they grow upward and finally coalesce with the frozen droplets.[125] Therefore, further studies should focus on the improvement of the water inhibition ability of the functional surfaces. In addition, they should also focus on standardizing the characterization methods for the heat transfer process to improve the icephobic performances of the SHSs.

Reduction in ice adhesion onto the solid surface

Once ice accumulates on the surface, an icephobic surface is required for the reduction of the adhesion strength so that the ice bulk can be easily removed with/without deicing operations. Generally, Van-der-Waals forces and electrostatic interactions contribute to the adhesion strengths between the ice bulk and most solid surfaces.[126] Also, the solid–ice separation often takes place at fractures, either in the ice itself or originating from interfacial defects.[127,128] Some studies have shown that the upper threshold of the pressure on the icephobic surface should not be larger than 10 kPa for a self-removal of the formed ice.[129] Most of the testing methods in the laboratory have been used to remove the ice and to measure the shear stresses in the solid–ice interfaces using force measuring probes[130] or centrifuges.[131] During the ice shear tests, the origin of the failures of the coated interfaces can be divided into five types, depending on where the failures occur.[132] The ice failures may occur at different locations, such as in internal sites of the ice layer, in ice coatings, in substrate–coating interfaces, and in mixed states. The tensile stress should also be evaluated,[43,133,134] although just a few studies have earlier been reported. Typically, if the distance between two bodies is within the attraction zone of the Van-der-Waals forces (≈0.5 nm), the adhesion of ice to the solid surface will be affected by the radius of the interacting area (R). When $R < R_{crit}$, the two contacting bodies are closely connected, which is called a shape independency. Otherwise, only a fraction of the two interacting bodies is in contact when $R > R_{crit}$, which is called a shape dependency. The critical radius (R_{crit}) of each substrate–ice contact point is formulated in the Griffith condition for crack initiation.[135]

Compared with superhydrophilic surfaces, the intermittent three-phase line on the SHSs can significantly reduce the solid–ice contact area, which is due to the trapped air in the surface micro/nanostructures.[77,136–138] However, the trapped air layer is not always well performing at low temperatures. One reason is that the water droplets will swell during the freezing process, which leads to an intrusion into the trapped air layer. Another reason is the relatively high humidity in a cold environment, which results in an accumulation of microsized water droplets in the micro/nanogaps (Figure 4e).[139,140] These droplets are required to overcome both the adhesive strength and the cohesive strength when mechanical interlocking takes place.[46] The factors that affect the solid–ice adhesion strength are the temperature and the equilibrium time of the ice surface layer.[141] The adhesion strength on the textured SHS increases when the temperature decreases. However, the actual ice adhesion strength can be decreased to several hours because of the latent heat release. During the water freezing process, metastable ice meniscuses are formed in the gaps of the surface texture, and the newly formed metastable meniscuses sublimate continuously.

To visualize the penetrations of the water droplets into the SHS, Tian et al.[115] observed a specific process at an increased temperature by using high-magnification charge-coupled detection. As revealed by cryo-scanning electron microscopy (cryo-SEM), the frost dendrites grow gradually until they are in contact with the iced droplets, which leads to a complete intrusion into the air pockets (Figure 4f). From the schematics of the substrate–ice contact situations, the internal contact regions illustrate an indirect contact within the ice–air interface. However, the frost bridge may further increase the ice adhesion, which is due to the gradual condensation of the tiny droplets. To minimize the influences of the ice bridge and frost propagation, the SHS should have good thermal conductivity, which leads to faster freezing of the mother droplets.[142] In addition, the localized cracks and the strain energy of the surface deformation are other factors that contribute to the interfacial toughness.[69,143] Golovin et al.[116] introduced low-interfacial toughness (LIT) materials and achieved good ice prevention, or ice strength-reduction performances, in large surface areas. As can be seen in Figure 4g, the removal forces in the solid–ice interface in the LIT material remain constant regardless of size of the iced area. This type of superhydrophobic coating material can effectively reduce the ice coverage on large flat aluminum panels, and in structures with complex geometries under real outdoor environment. In addition, Peyman et al.[144] presented a detachment method based on fast crack nucleation at the interfaces of fracture-controlled surfaces. The fast crack growth on fracture-controlled surfaces results in a weak adhesion of ice to the solid surface and a smaller energy consumption for shedding. From this perspective, icephobic surfaces with extremely weak ice adhesion strengths will be increasingly popular for future applications. Therefore, the surface textures should be carefully designed to prevent ice intrusion into the air pockets.

Inhibition of frost coverage

According to certain environmental conditions (such as a high temperature, high humidity, large droplet size, etc.), ice on surfaces often exhibits three types of structures. For water droplets with large diameters, the resulting glaze ice is the most common type of ice structure. In contrast, frost is formed when the water droplets have microscale sizes. It has a loose-structured morphology, like needles or feathers.[145] Also, the mixed ice is formed by water droplets with different diameters, with both glaze ice and frost characteristics. When considering

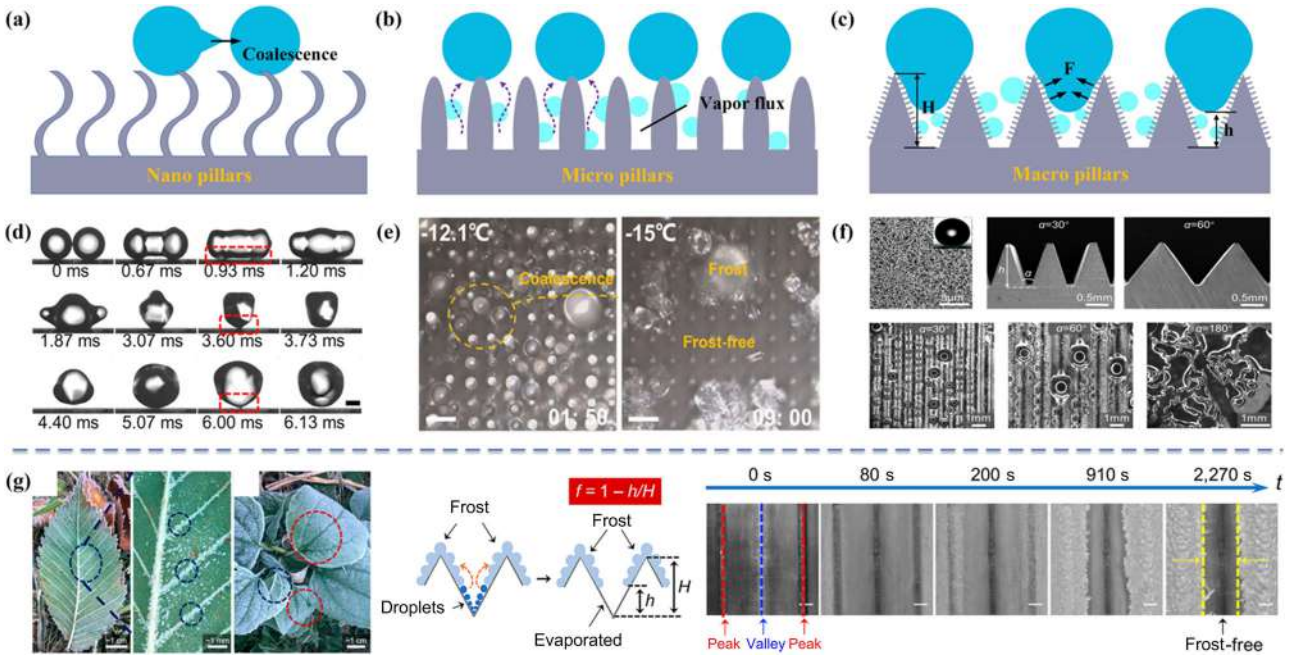

FIGURE 5 Controllable frost formations on representative superhydrophobic surfaces. Schematics of condensation processes on superhydrophobic surfaces with (a) nanopillars, (b) micropillars, and (c) macropillars. (d) Images of the coalesce of two neighboring droplets and the detachment process. Reproduced with permission.[148] Copyright 2019, American Chemical Society. (e) Condensation and frosting processes on surface microstructures. Reproduced with permission.[149] Copyright 2019, Royal Society of Chemistry. (f) Different condensation situations on macrotextured groove arrays. Reproduced with permission.[150] Copyright 2021, Elsevier. (g) Discontinuous frost patterns on natural leaves and 3D-printed artificial leaves, and a schematic of the frosting mechanism. Reproduced with permission.[151] Copyright 2020, National Academy of Sciences.

the topographical surface structure, frost formation on a SHS may show condensation, or direct deposition.[146,147] For SHSs with nanopillars, the condensed water droplets can repeatedly detach from the surfaces (Figure 5a). This detachment is driven by the energy release of the droplet coalescence.[152,153] As shown in Figure 5d, the coalesced droplets are detached from the surface when the initial and second droplets (and even more) reach a specific size.[148] The detachment behavior depends on the mismatch of droplet sizes, which is determined by the ratio of the diameters of two adjacent droplets. The detachment probability decreases when the radius of the smaller droplet increases. Consequently, an ice bridge is formed between deposited droplets, which leads to an interconnected ice growth phenomenon.[154] In addition, nanotextured surfaces are frost free even at high humidities, which is due to the vapor pressure in the nanocavities. Vercillo[155] discussed the relationship between the diameters of the droplets and the surface structure parameters (i.e., pillar-to-pillar distances and depths) by comparing the frozen sections under four different icing conditions. The results revealed that the Cassie-Baxter wetting state is preserved when these surface structure parameters are smaller than the diameters of the micrometric supercooled water droplets. For hierarchical micromorphologies, the textured SHSs are subject to a complete intrusion of frost (Figure 5b).[156] When the tiny droplets coalesce upward to the top of the micropillars, the released latent heats not only contribute to the evaporation of tiny condensates but also promote a coalescence of the droplets[149] (Figure 5e). From the in-plane dimension, the ice bridge occurs from the initial frozen drop and grows toward the evaporating liquid drop, resulting in the frost propagation.[157] It is roughly related to the ratio of interdrop distance to diameter of the evaporating liquid. For SHS, the value range of ratio is larger than traditional surfaces, leading to delay of the frost growth.[158] In addition, Graeber et al.[159] revealed that the ice/frost propagation was also influenced by local supersaturation and emission of a vapor bolus.

For macrotextured SHSs, the tiny water droplets continuous to condensate in the macrostructures. Due to the Laplace pressure that originates from the difference in curvatures, the condensed droplet spontaneously moves from the bottom to the top in the macrostructure when its volume keeps growing[150] (Figure 5c). In comparison with the flat SHSs, the microgroove structures prevent the 2D condensation of water. Instead, the water droplets are sliding in spherical shapes (Figure 5f). Similar frost prevention structures are found on natural leaves. Frost is easily formed on the veins on the backside of the leaf (i.e., convex side), but it is hardly formed on the veins on the front side (i.e., concave side) (Figure 5g). Inspired by this finding, Yao et al.[151] designed aluminum surfaces with serrated features on the millimeter scale. At low temperatures and high humidity levels, the supercooled droplets froze initially at the peaks of the surface structure without occupying the valleys. This was due to the vapor pressure difference and "ice bridge" effect. Therefore, careful control of the wettability of the SHS, size distribution of droplets, and surface topography are

effective in the inhibition of frost propagation.[160] Instead of using removal strategies, the promotion of self-coalescence of microsized droplets and self-repelling properties of the SHS are highly recommended for effective frost prevention. It is also necessary to systematically investigate the physical characteristics of water condensation and develop novel theories in the design of frost-free surfaces.

ICEPHOBIC LIQUID–LIQUID INTERFACE

In contrast to the solid–liquid–vapor three-phase interface on a SHS, the distinguishing feature of a slippery surface is the presence of lubricant meniscuses.[25,161,162] The slippery surface is a complex four-phase system involving solid, repelling liquid, lubricating liquid, and air phases. The oil–water spreading factor (S_{ow} (a)) is defined to describe the area between the water droplet and the oil.[84] For S_{ow} (a) < 0, the water droplet is entirely suspended by the oil layer, instead of being encapsulated. Therefore, the lubricant layer, with its low surface energy, provides the LIS with excellent icephobic properties. It is also essential to prevent the loss of the impregnated oil during the shedding process of the water droplet.

Frost/ice prevention properties

Liquid droplets easily condense when the water vapor is in contact with a surface at temperatures below the dew point. Once the liquid droplet is pinned to the exposed surface, the surface defects present a high hysteresis and immobilize the water droplet, which leads to an instant ice formation.[163] For SHSs, the tiny water droplets are prone to condensate at the surface defects. Slippery surface presents a better frost-/ice-free performance, where the hemispherical droplets that are formed by the coalescence of satellite droplets can sweep away the pinned droplets.[158,164,165] The microscale frost formation on the LIS involves complex dynamic processes: condensation, coalescence, growth, and propagation (Figure 6a). Weisensee et al.[17] demonstrated that the transition of water droplets depended on the critical nucleation radius (r_{min} = ~10–100 nm) and nucleation site density (N_s). Hence, the effective transition radius can be expressed as $r_e = 1/\sqrt{4N_s}$, and has a value in the range of ~0.5–10 μm. Once the water droplet reaches the maximum diameter (r_{max} = ~1 mm), it will slide off and "swallow" the droplets in the falling path if the gravitational forces overcome the pinning forces to the contact line. To improve the nucleation and removal rates of the water droplets, slippery surfaces have been designed by including various functions of bio-prototypes. Dai et al.[168] reported on a slippery rough surface where a hydrophilic lubricant was infused, which is designed from the inspiration of pitcher plants and rice leaves. It presented a superior vapor condensation performance and higher droplet mobility under capillary wetting and adequate drainage, which accelerated the droplet removal by gravity.

Moreover, the heat transfer on a LIS can be regarded as a system of thermal resistances that act on a single droplet. The dropwise heat transfer condensation can be modelled and the heat transfer rate (q_d) on the LIS can be expressed as shown in Equation 5[17]:

$$q_d = \frac{\Delta T_{tot}}{R_{tot}} = \frac{\Delta T_{tot} - \Delta T_c}{R_i + R_{cond} + R_s} \quad (5)$$

where ΔT_{tot} is the overall temperature difference, R_{tot} is the total thermal resistance, R_i is the interfacial resistance, R_{cond} is the conduction resistance, R_s is the structure resistance, and ΔT_c is the temperature change that is caused by the droplet curvature (i.e., the Kelvin effect). The total thermal resistance of the solid–liquid interface is related to the type of lubricant, surface micro/nanostructure (with height h_B), and energy of the surface coating (with thickness δ_{coat}). In addition, the growth speed and suction pressure of the frost contribute to the generation of a lubricant-depleted zone, which is directly influenced by the spacing between the micropillars (Figure 6b).[166] Thus, the frost-resistant property of the LIS is a synergistic effect of the lubricant and substrate morphologies.

Sliding dynamics

The dynamic prevention of water/ice on slippery surfaces is another effective icephobic method, where the water droplets slide off the surfaces by surface tension or by impacting momentum. For this situation, the physical properties of the infused lubricant should also be considered. Lee et al.[169] observed that the impact of water droplets on SHSs, and on surfaces infused with low-viscosity oils, presents rapid splashings. However, this is not the situation with surfaces infused with high-viscosity oils. This can be explained by the direct contacts in the solid–water interfaces, where the low viscous oils that are stored in the gaps are easily displaced by impacting water droplets. It is, therefore, essential to carefully select the lubricant type in the design of a slippery material for anti-icing applications. In addition, the thickness of the infused oil directly affects the homogeneity of the liquid distribution during the spreading-retracting process.[170] Hao et al.[171] found that a droplet that impacts a slippery liquid interface becomes completely rebound, which is similar to the dynamic process on a SHS. For the bouncing process, the interference fringe has been analyzed by reflection interference contrast microscopy, with a wavelength, λ, of 546 nm. This analysis has proved the existence of an intact air cushion at the interface.

To promote the water dynamic process, some studies have focused on disturbing the stability of the liquid–solid–liquid interface by tailoring the surface topography and characteristics of the lubricant. There are two representative studies on self-driven motions of water droplets on slippery surfaces. Sadullah et al.[167] constructed a topographical gradient on a textured substrate, where one side was a less dense section and the other a denser section. The water droplets spontaneously moved in either of two directions when the surface was infused with two different lubricants (ionic liquid and Krytox oil) (Figure 6d). These results showed that a combination of lubricants and topographical gradients is critical for a control of the force balance of the water droplets on a LIS. As illustrated in Figure 6c, the driving force reaches this balance under the interfacial tension between the

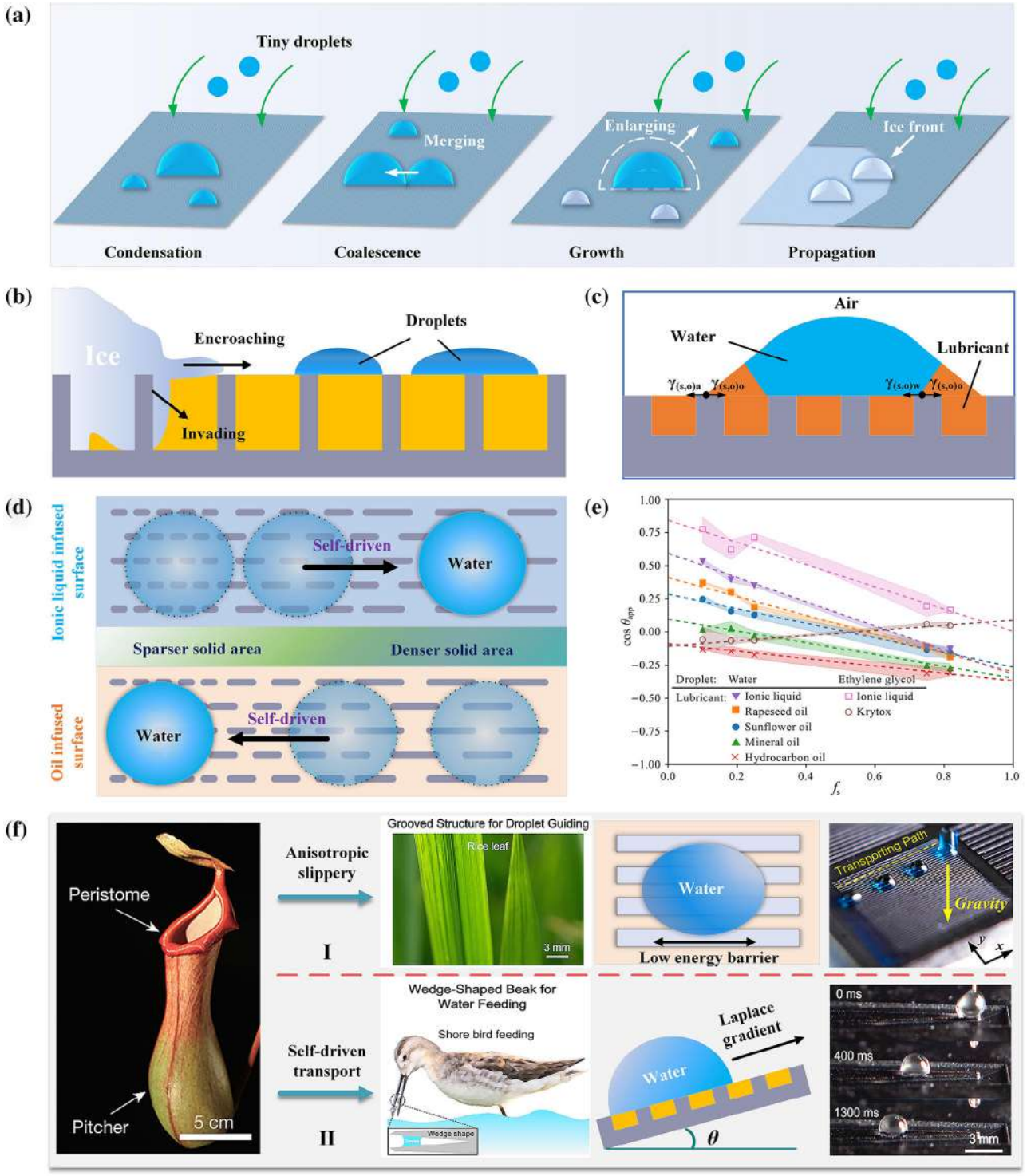

FIGURE 6 Dynamic prevention of water condensation and propagation on slippery surfaces. (a) Frost formation process on a LIS. (b) Schematic of a propagating frost front. Adapted with permission.[166] Copyright 2021, American Chemical Society. Schematics of the (c) meniscus area on a liquid-infused surface with a topographical gradient and (d) self-driven droplet motion. Adapted with permission.[167] Copyright 2020, Springer Nature. (e) Estimations of normalized driving forces. Reproduced with permission.[167] Copyright 2020, Springer Nature. (f) Combined strategies for anisotropic slippery situations: I. Sub-millimeter grooved structures like natural rice leaves; II. Wedge-shaped nanotextures like shorebird beaks. Reproduced with permission.[36,44] Copyright 2016, Springer Nature. Copyright 2021, American Chemical Society.

LIS and different phases (i.e., water ($\gamma_{(s,o)w}$), oil ($\gamma_{(s,o)o}$), and air ($\gamma_{(s,o)a}$)). Accordingly, the direction of the driving force ($\tilde{F}$) can be determined by Equation 6:

$$\tilde{F} = \left(\cos\theta^{\text{eff}}_{\text{wa|s}} - \cos\theta^{\text{eff}}_{\text{wa|o}}\right) \quad (6)$$

where $\theta^{\text{eff}}_{\text{wa|s}}$ and $\theta^{\text{eff}}_{\text{wa|o}}$ are defined as the contact angles of the droplets on a smooth solid surface and on a lubricant surface, respectively. The water droplets tend to move toward the denser solid area when $\theta^{\text{eff}}_{\text{wa|s}} > \theta^{\text{eff}}_{\text{wa|o}}$ since the solid part is easier wetted than the lubricant. Otherwise, the water droplets move in the opposite direction since the lubricant is preferably soaked. As can be seen in Figure 6e, the driving force is also varying when the surface is infused with different lubricants, which directly affects the water dynamics. Inspired by the water-feeding method of a shorebird beak, Yang et al.[44] fabricated wedge-shaped structures on SLIPS to obtain self-driven droplet transports. They, thereby, tailored the surface micro/nanotopography (Figure 6f). The continuous self-driven movement of droplets was achieved by the Laplace pressure gradients. The "footprints" of the droplets were then confined, and the bodies of the droplets were squeezed. The impelling forces were generated by the inner Laplace pressure gradients between the tail radii and head radii of the droplets. As can be seen in Figure 6f(II), the water droplets were squeezed to move along the wedges in a widening direction. When the 3D morphology of the submillimeter rice leaf-like grooved structure was altered, the droplets could, with the aid of gravity, be efficiently and precisely transported along the routes of the customized structure. This was attributed to the large difference in sliding resistance for the parallel and perpendicular directions with respect to the grooves, which is called the anisotropic slippery-Wenzel state (Figure 6f(I)). Therefore, the water droplets on this type of surface are most probably removed by themselves, or with the assistance of gravity, before being frozen. Thus, this surface has a high potential for applications in the anti-icing field.

Ice removal properties

As the air cushion is easily destroyed under harsh conditions, the SHSs become easily as worthless as icephobic surfaces. This situation leads to an increased ice adherence.[172,173] In contrast, when the air cushion is replaced by a lubricant, the lubricant forms a slippery surface and prevents the microscale water droplets from anchoring to the hierarchical surface structure. Consequently, the interfacial bonding on a slippery surface is a direct adhesion of ice to the lubricant (i.e., lubricant–ice interface) instead of a direct adhesion of ice to the solid surface (i.e., substrate–ice interface). Due to the low friction coefficient of the slippery surface, the ice can slip off the surface under a gentle external disturbance (like gravity or wind), even if the freezing droplets continuous to develop. This unique property makes the slippery surface a suitable candidate for anti-/deicing materials in high humidity environments.

As the most essential part of a slippery surface, the physical properties of different lubricants result in a difference in ice removal performances. The liquid oil is the most popular lubricant and has been used in many research studies. Due to the immiscibility of water and the oil lubricant, the tiny water droplets gradually deposit and coalesce on the lubricant film (Figure 7a). For slippery surfaces that are infused with the perfluorinated lubricant DuPont Krytox 100, the ice adhesion strength (~10 ± 7 kPa) is dramatically reduced compared with the fluorinated SHS at −40°C.[177] In Ref. 173, DuPont Krytox 103 was chosen as the lubricant fluid to decrease the evaporation rate of the lubricant layer. When coated with this lubricant, the unfrozen water on the surface of a turbine blade model was found to stream back along the blade structure more quickly than on an uncoated surface (Figure 7c). Due to the ultra-low ice adhesion strength (~35 kPa), the accumulated ice was more likely to sweep away by the incoming airflow, which led to a diminished ice formation. Additionally, silicone oil has also been selected as the infusing liquid, which is due to its nonvolatility and environmental-friendly properties. Long et al.[178] reported on a type of ultra-smooth solid–liquid interface that was infused with the silicone oil DC-200. The ice adhesion strength was as low as ~6.2 kPa. Furthermore, this lubricant functioned as a protective layer in cyclic freezing and drawing tests, thereby presenting good mechanical durability and a relatively long lifespan. Moreover, the quasi-liquid surface[174] is a new type of slippery surface that is based on silicone oil. One side of the grafted siloxane polymer chains is then tethered onto the substrate, while the other side is a free side (Figure 7b). This specifically layered structure not only improves the robustness of the slippery layer and substrate, but also secures a reduction in ice adhesion strength (26.1 kPa) at the extremely low temperature of −125°C (Figure 7d).

In addition to the oil lubricant, the slippery layer can also be a liquid water layer. As demonstrated in Figure 7e, the tiny water droplets are then completely absorbed by the water film. For example, Chen et al.[179] introduced a hygroscopic polymer network with water-swelling properties for the formation of a self-lubricating liquid water layer. This water layer demonstrated a low ice-adhesion strength (67 ± 8 kPa), even for temperatures lower than −25 °C. Furthermore, Dou et al.[38] prepared an anti-icing coating with an aqueous lubricating layer, for which the ice-adhesion strength was about 27 ± 6 kPa at a temperature of −53°C. Due to the good water adsorption properties of the hydrophilic pending groups, the covered ice was swept away by the wind at a speed of 12 m/s (Figure 7g).

When comparing the ice-adhesion strengths for two representative surfaces, the oil-infused lubricating surface presents a lower adhesion strength than the aqueous lubricating surface. However, the aqueous lubricating surface[180] shows the potential to remain robust in harsh environments because of the diminished leakage of lubricants. For example, Yao et al.[176] showed that propylene-glycol gel (PG-gel) uses the PG molecules as both a solvent and polymer network. The water diffusion in the PG-gel–ice interface enables the gel to contain a high-water concentration (Figure 7f), and a lubricant layer of a PG–H_2O mixture is formed between the PG-gel and ice. It has been shown that an ice cube can slide off the PG-gel surface even at a surrounding temperature of −40°C, which indicates a low adhesion strength to ice (Figure 7h). In addition, water droplets and ice crystals have been found to be hardly packed in the surface/ice interface. This type of

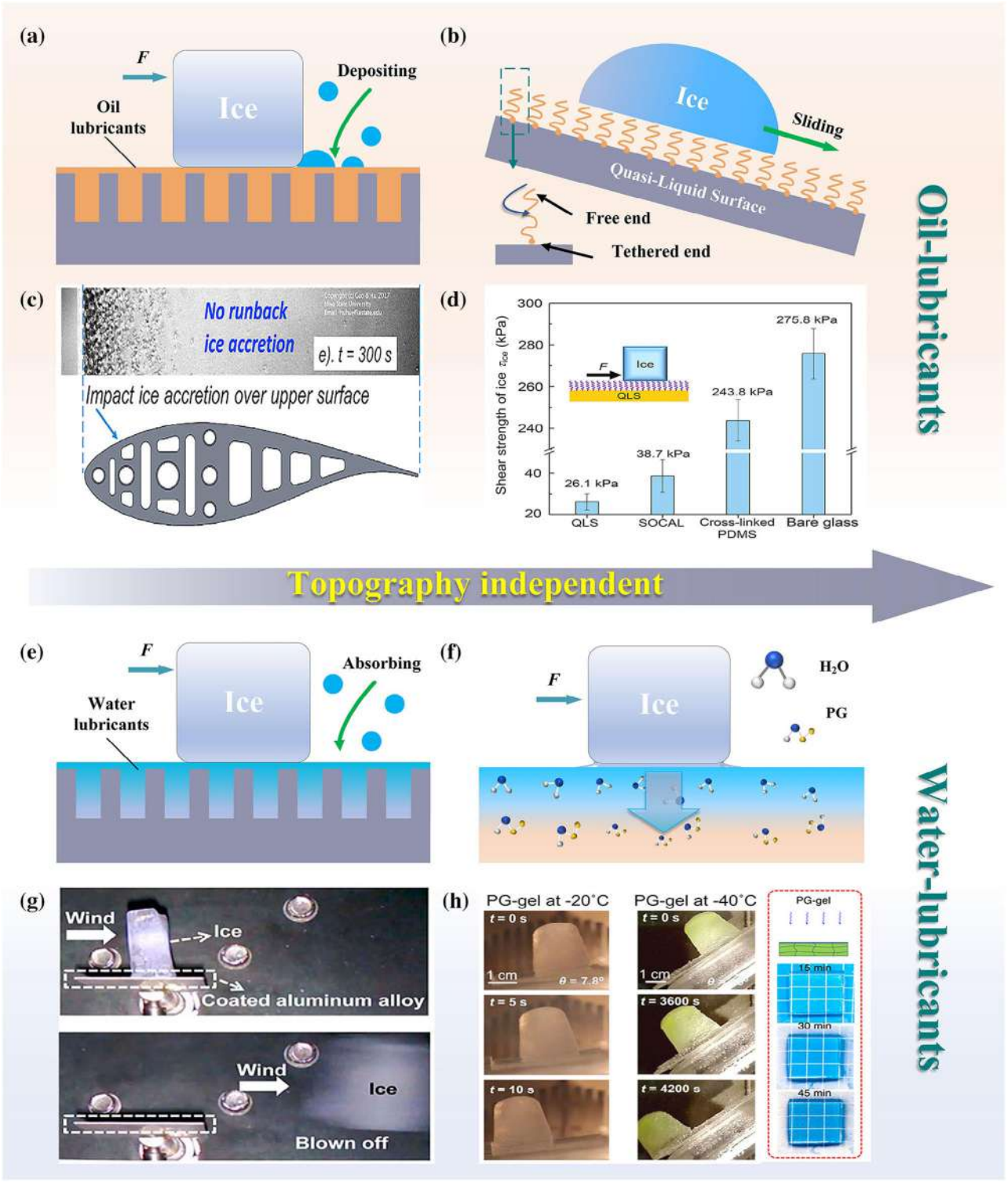

FIGURE 7 Ice removal performances of slippery surfaces with different types of lubricants. Schematics showing ice slippery on (a) an oil-lubricant surface and (b) a quasi-liquid surface. Adapted with permission.[174] Copyright 2020, American Chemical Society. (c) Ice formation on a turbine blade model coated with SLIPS. Reproduced with permission.[175] Copyright 2020, Elsevier. (d) Comparison of shear strengths of ice on representative samples. Reproduced with permission.[174] Copyright 2020, American Chemical Society. Schematics showing ice slippery on (e) a water-lubricant surface and (f) a PG-gel surface. Adapted with permission.[176] Copyright 2021, Elsevier. (g) Wind tunnel test of an aqueous lubricating layer. Reproduced with permission.[38] Copyright 2014, American Chemical Society. (h) Ice sliding performance on a tilted PG-gel surface at −20 and −40°C, respectively. Reproduced with permission.[176] Copyright 2021, Elsevier.

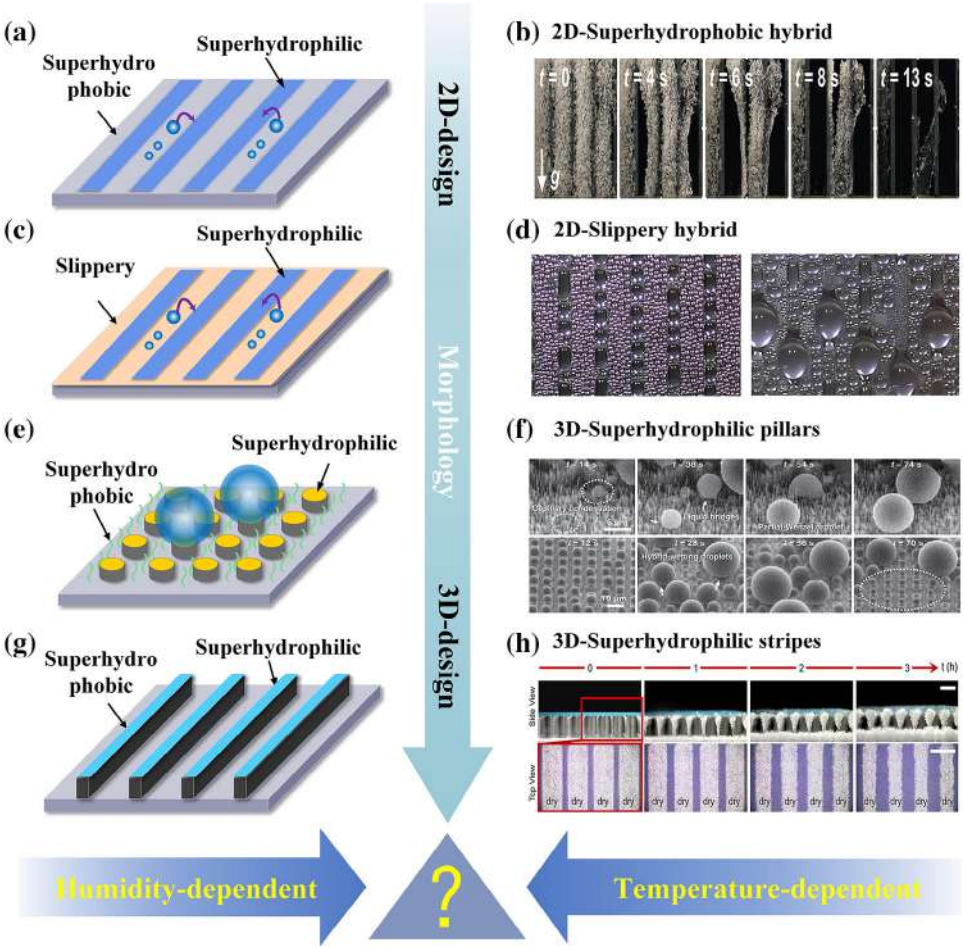

FIGURE 8 Frost prevention on patterned surfaces (a) Schematic and (b) evaluation of the dynamic defrosting performance of a 2D biphilic surface with superhydrophobic and superhydrophilic properties. Reproduced with permission.[181] Copyright 2020, Elsevier. (c) Schematic and (d) process of water condensation on a biphilic quasi-liquid surface. Reproduced with permission.[182] Copyright 2023, Wiley-VCH. (e) Schematic and (f) evaluation of the dynamic defrosting performance of a 3D biphilic surface. Reproduced with permission.[183] Copyright 2018, American Physical Society. (g) Schematic and (h) frosting condensation process on an ice-patterned aluminum surface. Reproduced with permission.[184] Copyright 2018, American Chemical Society.

material thereby shows an improved antifrost property as compared with oil-infused porous materials and superhydrophobic materials. In addition, the aqueous lubricating film keeps the PG-gel interface transparent during the icing process, thereby showing a high potential for transparency-required applications (such as solar panels, windows, and eyeglasses). Therefore, the physical properties of lubricants play a significant role in the promotion of ice removal performances, and the lubricants can also be designed with robustness and a long lifespan for real applications.

HYBRID METHODS FOR ICEPHOBICITY

Although superhydrophobic and LISs have been listed as promising candidates for icephobic applications, simple interfacial characteristics, or strategies, are insufficient for the prevention of ice coverages on substrates under extreme conditions. For SHSs, the air cushions are very fragile at low temperatures and high humidities. They can be quickly replaced by tiny water droplets. Also, the LISs are subject to lubricant leakages, which result in short lifespans. Recently, some hybrid methods have been proposed to further improve the icephobic properties.

Patterned surfaces

One approach is to create regular forms of hybrid wettability on the surfaces, like the wetting state of Namib Desert Beetles. The surface topography and wettability are two important parameters for this strategy. To achieve an excellent icephobic performance, 2D (or 3D) biphilic surfaces with hybrid wettability have been designed and their surface wettability has been optimized. For surfaces with 2D superhydrophobic and superhydrophilic properties, the water droplets prefer to condense on the superhydrophilic areas while they spontaneously adsorb on the superhydrophobic areas. As illustrated in Figure 8a, this leads to an easy removal of ice/frost. Gurumukhi et al.[181]

presented dynamic defrosting properties of branched biphilic surfaces by designing the hybrid wettability on the same type of surface, but horizontally (Figure 8b). This work was inspired by the vein network patterns on banana leaves.[185] These biphilic patterns are composed of regular parallel hydrophilic trunks and triangular branches. In the defrosting process, the ice slush in the superhydrophobic areas moves first to the hydrophilic branches, followed by a lateral movement to the hydrophilic trunks. This is due to the Laplace pressure gradients in the different channels. Interestingly, the ice slush is then gradually lifted off from the superhydrophobic area by the coalescence in the hydrophilic area. In the meantime, the water and slush passively flow toward the trunk under capillary pumping forces, which results in a quick cleaning of the superhydrophobic regions. When replacing the material in the superhydrophobic regions with a slippery material, the water droplets coalesce and grow rapidly before sliding off from the surface (Figure 8c). As inspired by beetles, Boylan et al.[182] reported on water coalescence performances on biphilic quasi-liquid surfaces. During the coalescing process, the droplets migrated from the hydrophobic regions to the hydrophilic regions, which led to rapid droplet removal by the sweep-off of large droplets from the surfaces (Figure 8d).

Moreover, biphilic surfaces with 3D morphologies are generally designed with hydrophilicities on top of the pillars, or ridges (Figures 8e and g, respectively). For example, Hou et al.[183] created a type of biphilic surface with hydrophilic micropillar arrays and superhydrophobic nanograss, and they investigated the nucleation rate of frost. The droplets condensed and grew gradually on the hydrophilic micropillars, which was caused by the low water nucleation barrier. The ice nuclei were significantly inhibited when the water droplets exceeded their critical radii (Figure 8f). This unique characteristic can contribute to a quick shed-off of nucleated water droplets by the wind or gravity. In addition, Li et al.[133] showed that water droplets spread asymmetrically before reaching their maximum diameters on biphilic surfaces, instead of being symmetrical spread on SHSs. In the recoiling process, the flattened droplet is torn into fragments because of the variation in surface tension ($\gamma_{superhydrophilic} > \gamma_{superhydrophobic}$). These characteristics are beneficial for the reduction of the solid–liquid contact time and inhibit the accumulation of frozen droplets. For surfaces with linear striped patterns, Ahmadi et al.[184] discussed the antifrosting performances of periodic hygroscopic arrays (called sacrificial ice stripes). These arrays can effectively obtain frost-free regions between the sacrificial ice stripes on intermediate surface areas (Figure 8h). The neighboring moisture is attracted solely to the top of the stripes because of the decreased vapor pressure. In addition, the coarsening ice remains in the "Cassie" state without overlapping with the adjacent ice stripes, so the ice stripes will be quickly removed. Similarly, Jin et al.[186] showed that the patterned polyelectrolyte brush (PB) can achieve up to 96% of ice-free regions by tuning the ice nucleation and propagation. By using phase-change materials, the latent heat is simultaneously released during the ice formation process. Finally, the water droplets in the regions between the PBs evaporate and the ice bridge formation during propagation is significantly inhibited. Consequently, the icephobic performances of biphilic surfaces are predominantly temperature and humidity dependent. For future research, it is hereby suggested to focus on the design of biphilic surfaces with various topographies and to reveal the corresponding coalescence mechanisms.

Smart interfaces

Penguins are good at preventing ice adhesion although living in an extremely cold environment. They have developed two distinct ways to be free from ice.[187] One way is to shed the water before it is frozen, which is achieved by the air cushion formed by the microstructures of the feathers. The other way is to shed the ice by forming a type of preen oil coating on the nanostructures of the feathers. Consequently, surfaces that are designed with the capability to reversibly switch from superhydrophobicity to slippery properties (Figure 9a) show great potential for icephobic applications. Li et al.[25] constructed a rough SHS by using a spray coating method, which was further developed into a slippery surface by dodecane infusion. Once the slippery surface was washed with ethanol, it recovered to a superhydrophobic performance. The superhydrophobic and slippery performances were well preserved after nine cycles of infusion-washing. As a result of anti- and deicing tests, both surfaces presented good water repellencies and ice removal performances in a cold environment. Wang et al.[192] used a laser ablation method in fabricating a slippery-superhydrophobic switchable surface. Due to environmental disturbances, the surface was able to adaptively create a slippery state, or superhydrophobic state, with good icephobic functions.

Another popular way is to combine the active and passive methods.[193–195] Based on the nonadhesive performance of the superhydrophobic, or slippery, surface, the ice prevention and removal properties can be significantly improved by coupling with the electro-, or photo-, thermal effect[196–198] (Figures 9d and e, respectively). The electrothermal strategy is a simple way to fabricate two layers that consist of a functional layer and an electrothermal layer, respectively. For example, Wan et al.[199] proposed a method to combine the self-lubricating layer and the electrothermal layer. Combined with the low friction coefficient, the ice adhesion strength could be further reduced under Joule heat. In addition, the phase-change materials that can be regulated with electrothermal layers are popular and have also been used in icephobic applications. Wang et al.[188] proposed a flexible composite film that consisted of a graphite coating, paraffin wax, and parallel copper foil electrodes. This composite film demonstrates a reversible transition of the lubricant from the solid phase (i.e., pseudo-slippery state) to the liquid phase (i.e., slippery condition), which can be altered by the temperature. When heating the paraffin wax above its melting temperature, the slippery surface enables the cool droplets to slide off and, thereby, prevent ice formation (Figure 9b). The energy consumption can be considerably lowered by self-regulating the temperature system. In addition, the icephobic materials can be smarter if the accumulation of water, or ice, is carefully detected. Zahra et al.[200] constructed a hybrid deicing system by embedding a microwave resonator sensor and periodic heaters simultaneously. As a result, the ice formation on the surfaces could be precisely detected and efficiently

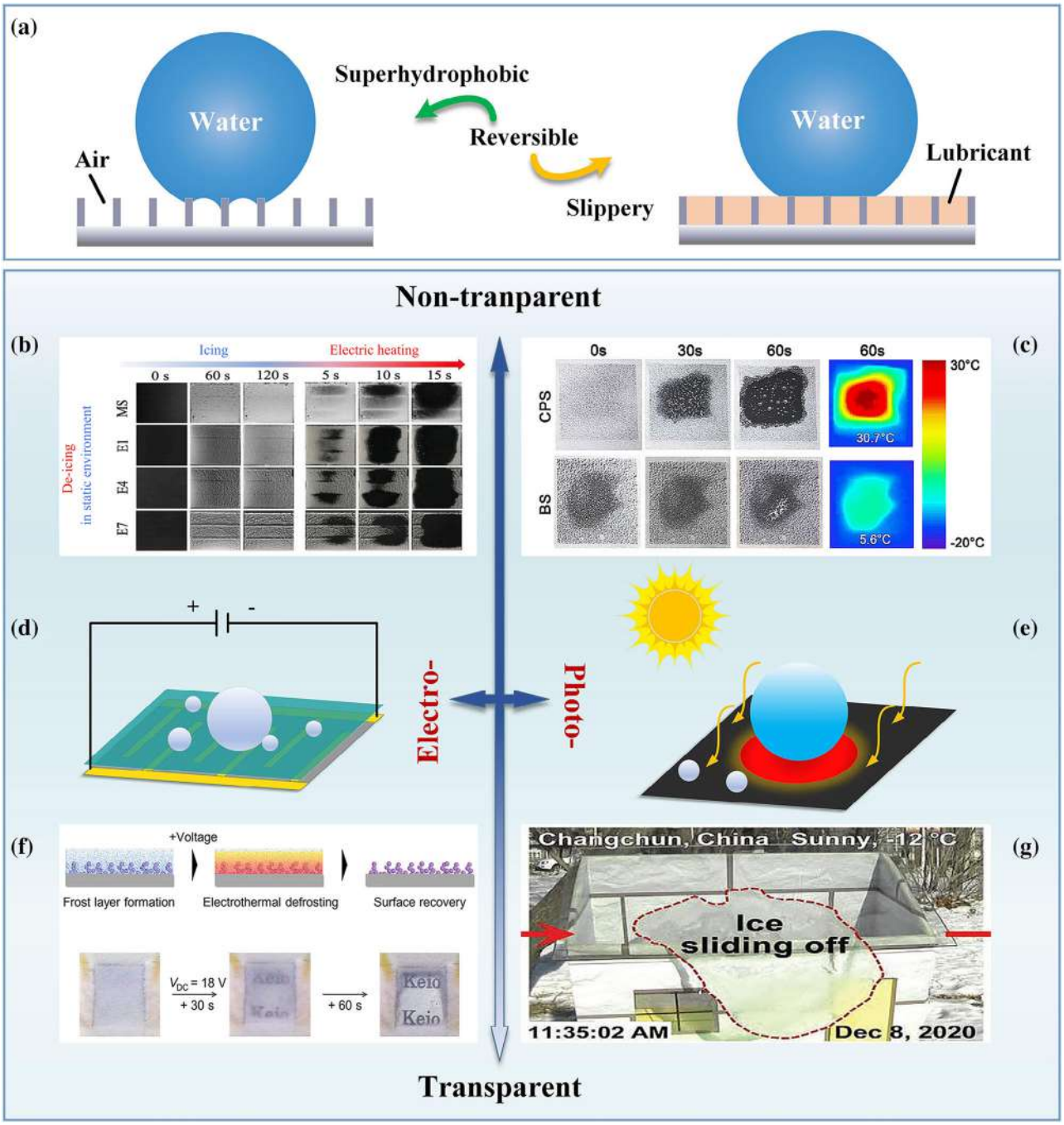

FIGURE 9 Ice prevention and removal behavior of smart interfaces. (a) Schematic of smart control of interfacial wettability. (b) Images of ice formation and deicing processes on electrothermal composite film. Reproduced with permission.[188] Copyright 2022, Elsevier. (c) Photothermal and ice-melting properties of carbon nanoparticle coatings. Reproduced with permission.[189] Copyright 2021, American Chemical Society. Schematics of the (d) electric heating process and (e) light-to-heat process, respectively. (f) The voltage-induced electrothermal defrosting process on a superhydrophobic transparent coating. Reproduced with permission.[190] Copyright 2016, American Chemical Society. (g) The solar deicing process on an MXene-SOPS-coated glass. Reproduced with permission.[191] Copyright 2022, Wiley-VCH.

removed, which led to a dramatic reduction in energy consumption. In addition, transparency is another characteristic that should be considered in the design of icephobic materials. However, transparent electrothermal materials are relatively difficult to fabricate, which is due to the high transparency requirements. Matsubayashi et al.[190] prepared transparent superhydrophobic composite films with good electrical conductivities by using ethylene glycol treatments. As can be seen in Figure 9f, frost on these surfaces is quickly removed at low voltages and low environmental temperatures. Therefore, the hybrid surfaces, which consist of a combination of functional surfaces and electro-heaters, provide facilities with an excellent repulsion of freezing rain at the anti-icing stage and a rapid ice/frost-melt performance at

the deicing stage by using Joule heat. The challenge, however, is to uniformly embed the electro-heaters into the materials without degrading other functions.

Photo-thermal methods utilize the excellent light absorption properties of microparticles/fibers to increase the temperatures at the interface,[173,201–204] which is both environmentally and economically friendly. Carbon is the most common photothermal material that can be rapidly heated under near-infrared (NIR) irradiation. This is due to its high photothermal conversion efficiency, which is a very important factor.[205,206] As can be seen in Figure 9c, the deposited frost/ice on the superhydrophobic photothermal surface rapidly melts and converges into water droplets. For example, Jiang et al.[207] coated superhydrophobic carbon nanoparticles (CNPs) on ethylene vinyl acetate substrates, which showed good photothermal efficiencies (of 50.94%) in deicing tests. Although the CNPs present excellent deicing performances, it may be difficult to prepare the CNPs industrially. Yang et al.[189] developed a continuous roll-to-roll system for fabricating CNPs from candle soot with enhanced productivity. The photothermal materials were prepared by spraying CNPs on untreated PDMS layers for large-scale applications. In addition, this is also a good method for developing photothermal solid slippery surfaces.[208] The nanoparticles on the substrates can largely increase the surface temperatures under NIR illumination, leading to phase changes in the solid lubricants. More importantly, the melted liquid lubricant accelerates the slippery capacity of the melted ice. However, there are few research reports on transparent photothermal materials. The reason is that it is difficult to achieve light-to-heat properties and transparency simultaneously.[209,210] To achieve photothermal and transparency properties, MXenes are the best candidates for the replacement of other types of carbon materials.[211,212] Niu et al.[191] developed a transparent self-healable solar anti-/deicing surface of MXene, which was assembled layer-by-layer. It showed a high transmittance larger than 77% at a wavelength of 550 nm. After coating with the solid lubricant, the MXene multilayers could quickly shed off the unfrozen water and melted ice/frost (Figure 9g). As discussed above, smart interfaces that respond to external stimuli will be the next popular trend in the design of icephobic materials with less energy consumptions.

Smart substrates

Icephobic materials can also be designed with structural deformations of smart substrates in response to external stimuli. Plants and animals have inspired potential solutions to the existing drawback of artificial icephobic surfaces, and these surfaces can be considered as smart systems. Thus, it can be foreseen that smart systems are able to remove the ice by deforming the substrates at a micro/macroscale, which is driven by external stimuli.[213] For SHSs with microscale deformations, the micropillars are expected to rapidly change their shapes and release energies for the shedding of adhered water/ice (Figure 10a). By using the shape memories of polymers, Shao et al.[214] reported on a controllable droplet adhesion onto smart SHSs (Figure 10c). With a precise illumination with NIR light, the adhered water was released and rolled off the surfaces, which was caused by the shape recoveries of the microstructures. Moreover, mimosa pudica is a plant with ciliates that can quickly fold its leaflets in response to a slight contact pressure.[220] Inspired by this rapid cascadefolding mechanism, the superhydrophobic substrates show excellent water/ice repellency performances with macrodeformation abilities (Figure 10b). For example, Kamran et al.[195] developed a passive deicing system with a low ice adhesion strength, which could remove the ice by pressing air into the channels, or by melting the ice by heating the air in the channels. As can be seen in Figure 10d, the ice bulk was bounced off from the surface under a pressure of 21 kPa. Therefore, once combined with pneumatic systems, the icephobic performances can be significantly improved on superhydrophobic substrates with transformation capacities.

For smart slippery surfaces, it is a good strategy to store the antifreeze lubricants within the microstructures of the substrates, which are then released under the action of a combination of stimuli[221,222] (like temperature,[223,224] stress,[225] light,[226] electrical field,[227] and magnetic field[228]) (Figure 10e). As an example, the poisonous dart frog continuously produces mucus through special glands to keep its skin hydrated (Figure 10g).[216,229] Inspired by its bilayer skin architecture, Wang et al.[217] constructed solid organogel materials by diffusing melted alkanes into crosslinked poly(dimethylsiloxane), which thereby underwent swelling. This solid organogel consists of a particle-embedded layer, a boundary layer, and a pure alkane layer. If the alkane layer is damaged, or removed, the alkane molecules continue to diffuse in an outward direction, which is caused by the concentration gradient and the stress. They can, thereby, form an alkane crystalline layer with excellent icephobic durability. Furthermore, the smart slippery substrates should be provided with macroscale transformation capabilities for the improvement of ice removal performances (Figure 10f). Furthermore, earthworms show a similar self-lubricating mechanism when passing through cohesive soil[218] (Figure 10h). Its slippery layer can prevent the skin from coming in contact with soil particles, and demonstrates friction reduction, wear resistance, and self-cleaning properties. The mucus is secreted in the soil to cover the rough skin with macroscopic annuli and microripples. Similar to this mechanism, Irajizad et al.[219] discussed the dynamic motion of ice on magnetic slippery surfaces with low ice adhesion strengths (≈2 Pa). Thus, the development of smart materials provides a promising way to design smart functional substrates that can effectively remove ice under extreme conditions.

CONCLUSIONS AND OUTLOOKS

A new concept of smart systems inspired by animals and plants has been proposed in the present review, which is expected to be the best icephobic candidates for future applications. By illustrating smart prevention mechanisms, the wetting characteristics of representative species (like plants, insects, birds, and fishes) have then been compared and discussed. For a living organism, the specific wettability not only depends on the surface morphology and chemicals, but also on the smart responsive ability in contact with the surrounding. Furthermore,

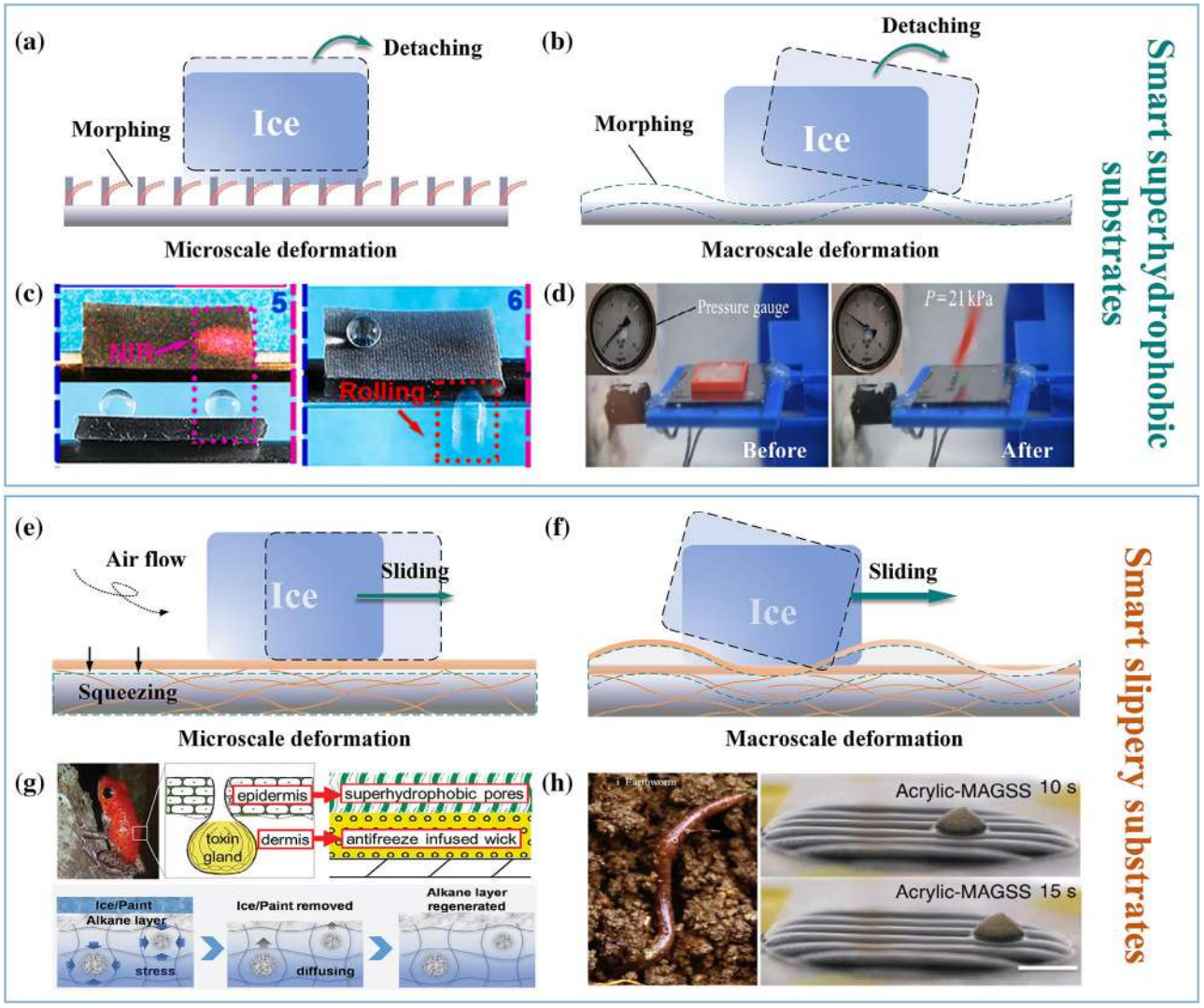

FIGURE 10 Potential ice removal strategies for smart substrates. Schematics of ice removal on smart superhydrophobic substrates with (a) microdeformations and (b) macrodeformations. (c) Controllable droplet removal by NIR light. Reproduced with permission.[214] Copyright 2022, Wiley-VCH. (d) An active deicing system by using a pneumatic method. Reproduced with permission.[215] Copyright 2017, Wiley-VCH. Schematics of ice removal on smart slippery substrates with (e) microdeformations and (f) macrodeformations. (g) Stimuli-responsive antifreeze coatings like frog skin. Reproduced with permission.[216,217] Copyright 2015, Wiley-VCH. Copyright 2017, Wiley-VCH. (h) Icephobic performance of a magnetic slippery surface like an earthworm. Reproduced with permission.[218,219] Copyright 2018, Wiley-VCH. Copyright 2016, Springer Nature.

anti-/deicing mechanisms on SHSs and slippery surfaces have been elaborated with respect to dynamic properties, nucleation, and heat transfer theories, in addition to theories of interface mechanics. It can be summarized that the air cushion in the solid–liquid–air interface can propel the water dynamic impact, inhibit the nucleation of ice, and reduce the ice adhesion strength, even though it may be fragile.[33,34] If the air cushion is replaced by a liquid, the resulting slippery surface has the potential to undertake the intrusion of water droplets, where water/ice is easily sliding off.[230] The constant liquid–liquid line can effectively prevent the coverage of microscale water droplets.

Consequently, smart interfaces and smart substrates are two essential characteristics in intelligent icephobic systems, by which it is possible to inhibit, or remove, ice in response to an external stimulus (like heat,[213] light,[231] magnetic field,[128] and electricity[206,232]). Smart interfaces play an essential role in anti-icing and deicing processes. They are designed with smart repellence, or switchable wetting, properties in response to multiscale water, or ice, in anti-icing processes.[216,233,234] For instance, interfaces can be designed with phase-change properties under external stimuli. The encapsulated phase-change material presents a good ice-delaying performance by automatically releasing latent heat during solidification, which results in a higher surface temperature.[42] In addition, the phase-change of lubricants (i.e., from solid to liquid), in response to stimuli, provides a new layer of slippery film to facilitate the ice removal process. Therefore, smart interfaces will function as shield protection components that are free from ice damage. Smart substrates can be designed to change their shapes under external stimuli, thereby promoting the detachment of ice/frost. The development of smart materials has made

it possible to modify the deformation of substrates, including magnetostrictive materials, electroactive polymers, shape memory alloys, and SMPs. As an example of representative smart materials, SMPs[235–238] are good candidates for smart deicing applications, which is due to the typical features of shape-change and variable stiffness in response to external stimuli. By introducing functional particles, or fibers, composites of SMPs can be included in more complex actuation methods and deformation capacities, extending the flexibility of their icephobic applications.[239–241] Given that a direct detachment may cause severe damage to surface structures, it has been suggested to integrate smart interfaces and substrates in the design of intelligent icephobic systems. Deformations of a combined smart interface and substrate can quickly result in ice removal performances.

It is expected that there will be a demand for smart icephobic systems in the future. The development of smart materials will provide a vast number of fundamental materials for the construction of smart icephobic systems. In addition, corresponding theories about smart icephobic systems should be established as guidance for the design and optimization of related processes. It is also necessary to unify standard tests and establish testing equipment to evaluate the icephobic performances[180,242] (such as nucleation time, ice adhesion strength, and frost prohibition capacity). This may help in the development of icephobic theories and in the design of novel icephobic materials. For industrial applications, robustness tests are another aspect that should be emphasized. The methodologies of mechanical, chemical, and environmental measurements are preferably introduced based on American Society for Testing and Materials (ASTM) or International Organization for Standardization (ISO) standards.[243] For practical applications, durability and robustness are the main challenges for smart icephobic systems. It is, therefore, necessary to construct smart icephobic systems with low cost and extended lifespan properties. This review has provided some insights into the design of novel smart icephobic systems, which can be useful for the promotion of potential applications in the future.

ACKNOWLEDGMENTS

This work was supported by the following funds: National Natural Science Foundation of China (No. 12102105), China Postdoctoral Science Foundation (No. 2021M690834), Postdoctoral Science Foundation of Heilongjiang Province (No. LBH-Z21156), and Foundation for Innovative Research Groups of the National Natural Science Foundation of China (No. 52021003).

CONFLICT OF INTEREST STATEMENT

The authors declare no conflict of interest.

ORCID

Yanju Liu https://orcid.org/0000-0001-8269-1594

REFERENCES

1. Shijin W, Yuande Y, Yanjun C. Global snow-and ice-related disaster risk: a review. *Nat Hazards Rev*. 2022;23:3122002.
2. Brassard J, Blackburn C, Toth M, Momen G. Ice accretion, shedding, and melting on cable-stayed bridges: a laboratory performance assessment. *Cold Reg Sci Technol*. 2022;204:103672.
3. Maloney TC, Diez FJ, Rossmann T. Ice accretion measurements of jet a-1 in aircraft fuel lines. *Fuel (Lond)*. 2019;254:115616.
4. Zhang Y, Wang J, Jiang C, et al. Investigation of ice and snow accumulations on the bogie areas of high-speed trains using ice wind tunnel experiments. *Cold Reg Sci Technol*. 2022;199:103560.
5. Barker AJ, Douglas TA, Alberts EM, et al. Influence of chemical coatings on solar panel performance and snow accumulation. *Cold Reg Sci Technol*. 2022;201:103598.
6. Giappino S, Rocchi D, Schito P, Tomasini G. Cross wind and rollover risk on lightweight railway vehicles. *J Wind Eng Ind Aerodyn*. 2016;153:106-112.
7. Rønneberg S, Laforte C, Volat C, He J, Zhang Z. The effect of ice type on ice adhesion. *AIP Adv*. 2019;9:55304.
8. Wei W, Ni L, Wang W, Yao Y. Experimental and theoretical investigation on defrosting characteristics of a multi-split air source heat pump with vapor injection. *Energy Build*. 2020;217:109938.
9. Yang Q, Zhang Z, Yang S, et al. Study on the characteristics of water jet injection and temperature spatial distribution in the process of hot water deicing for insulators. *Energies (Basel)*. 2022;15:2298.
10. Xia Q, Zhang Z, Liu Y, Leng J. Buckypaper and its composites for aeronautic applications. *Compos Part B: Eng*. 2020;199:108231.
11. Wang Y, Xu Y, Su F. Damage accumulation model of ice detach behavior in ultrasonic de-icing technology. *Renew Energy*. 2020;153:1396-1405.
12. Wei K, Yang Y, Zuo H, Zhong D. A review on ice detection technology and ice elimination technology for wind turbine. *Wind Energy (Chichester)*. 2020;23:433-457.
13. Zhang X, Chen J, Zhan L, et al. Study on groundwater recharge based on chloride mass balance and hydrochemistry in the irrigated agricultural area, north China plain. *Environ Earth Sci*. 2023;82:70.
14. Ramakrishna DM, Viraraghavan T. Environmental impact of chemical deicers—a review. *Water Air Soil Pollut*. 2005;166:49-63.
15. Xu G, Shi X. Impact of chemical deicers on roadway infrastructure: risks and best management practices. In: Shi X, Fu L, eds. *Sustainable Winter Road Operations*. John Wiley & Sons Ltd.; 2018:211-240.
16. Yang S, Wu C, Zhao G, et al. Condensation frosting and passive anti-frosting. *Cell Rep Phys Sci*. 2021;2:100474.
17. Weisensee PB, Wang Y, Qian H, et al. Condensate droplet size distribution on lubricant-infused surfaces. *Int J Heat Mass Transf*. 2017;109:187-199.
18. Miao S, Liu X, Chen Y. Freezing as a path to build micro-nanostructured icephobic coatings. *Adv Funct Mater*. 2023;33:2212245.
19. Ouyang M, Guo R, Fan Y, et al. Ultralow-adhesion icephobic surfaces: combining superhydrophobic and liquid-like properties in the same surface. *Nano Res*. 2023;16:589-598.
20. Chatterjee R, Bararnia H, Anand S. A family of frost-resistant and icephobic coatings. *Adv Mater*. 2022;34:2109930.
21. Wohl CJ, Berry DH. *Contamination Mitigating Polymeric Coatings for Extreme Environments*. Springer; 2019.
22. Del Moral J, Montes L, Rico-Gavira VJ, et al. A holistic solution to icing by acoustic waves: de-icing, active anti-icing, sensing with piezoelectric crystals, and synergy with thin film passive anti-icing solutions. *Adv Funct Mater*. 2023;33:2209421.
23. Liu Y, Wu Y, Liu S, Zhou F. Material strategies for ice accretion prevention and easy removal. *ACS Mater Lett*. 2022;4:246-262.
24. Jiang S, Diao Y, Yang H. Recent advances of bio-inspired anti-icing surfaces. *Adv Colloid Interface Sci*. 2022;308:102756.
25. Li X, Zhao Z, Liu Y, Liu Y, Leng J. Smart controlling on the bistable state of bio-inspired multifunctional coatings for anti-/de-icing applications. *Prog Org Coat*. 2023;183:107754.

26. Feng L, Li S, Li Y, et al. Super-hydrophobic surfaces: from natural to artificial. *Adv Mater*. 2002;14:1857-1860.
27. Ma M, Hill RM. Superhydrophobic surfaces. *Curr Opin Colloid Interface Sci*. 2006;11:193-202.
28. Bhushan B, Jung YC. Natural and biomimetic artificial surfaces for superhydrophobicity, self-cleaning, low adhesion, and drag reduction. *Prog Mater Sci*. 2011;56:1-108.
29. Li M, Li C, Blackman BR, Eduardo S. Mimicking nature to control biomaterial surface wetting and adhesion. *Int Mater Rev*. 2022;67:658-681.
30. Liu Y, Andrew M, Li J, Yeomans JM, Wang Z. Symmetry breaking in drop bouncing on curved surfaces. *Nat Commun*. 2015;6:10034.
31. Feng X, Zhang X, Tian G. Recent advances in bioinspired superhydrophobic ice-proof surfaces: challenges and prospects. *Nanoscale*. 2022;14:5960-5993.
32. Li D, Ma L, Zhang B, Chen S. Facile fabrication of robust and photothermal super-hydrophobic coating with efficient ice removal and long-term corrosion protection. *Chem Eng J*. 2022;450:138429.
33. Erbil HY. Practical applications of superhydrophobic materials and coatings: problems and perspectives. *Langmuir*. 2020;36:2493-2509.
34. Jung S, Dorrestijn M, Raps D, et al. Are superhydrophobic surfaces best for icephobicity? *Langmuir*. 2011;27:3059-3066.
35. Varanasi KK, Deng T, Smith JD, et al. Frost formation and ice adhesion on superhydrophobic surfaces. *Appl Phys Lett*. 2010;97:234102.
36. Chen H, Zhang P, Zhang L, et al. Continuous directional water transport on the peristome surface of nepenthes alata. *Nature*. 2016;532:85-89.
37. Xu W, Wang Z. Fusion of slippery interfaces and transistor-inspired architecture for water kinetic energy harvesting. *Joule*. 2020;4:2527-2531.
38. Dou R, Chen J, Zhang Y, et al. Anti-icing coating with an aqueous lubricating layer. *ACS Appl Mater Interfaces*. 2014;6:6998-7003.
39. Ma J, Pan W, Li Y, Song J. Slippery coating without loss of lubricant. *Chem Eng J*. 2022;444:136606.
40. Rykaczewski K, Anand S, Subramanyam SB, Varanasi KK. Mechanism of frost formation on lubricant-impregnated surfaces. *Langmuir*. 2013;29:5230-5238.
41. He Z, Wu C, Hua M, et al. Bioinspired multifunctional anti-icing hydrogel. *Matter*. 2020;2:723-734.
42. Yancheshme AA, Allahdini A, Maghsoudi K, et al. Potential anti-icing applications of encapsulated phase change material–embedded coatings: A review. *J Energy Storage*. 2020;31:101638.
43. Li X, Wang G, Moita AS, et al. Fabrication of bio-inspired non-fluorinated superhydrophobic surfaces with anti-icing property and its wettability transformation analysis. *Appl Surf Sci*. 2020;505:144386.
44. Yang X, Zhuang K, Lu Y, Wang X. Creation of topological ultraslippery surfaces for droplet motion control. *ACS Nano*. 2020;15:2589-2599.
45. Wang L, Tian Z, Jiang G, et al. Spontaneous dewetting transitions of droplets during icing & melting cycle. *Nat Commun*. 2022;13:378.
46. Chen J, Liu J, He M, et al. Superhydrophobic surfaces cannot reduce ice adhesion. *Appl Phys Lett*. 2012;101:111603.
47. Neinhuis C, Barthlott W. Characterization and distribution of water-repellent, self-cleaning plant surfaces. *Ann Bot*. 1997;79:667-677.
48. Hallam ND. Growth and regeneration of waxes on the leaves of eucalyptus. *Planta*. 1970;93:257-268.
49. Koch K, Bhushan B, Barthlott W. Diversity of structure, morphology and wetting of plant surfaces. *Soft Matter*. 2008;4:1943-1963.
50. Zang D, Zhu R, Zhang W, et al. Corrosion-resistant superhydrophobic coatings on mg alloy surfaces inspired by lotus seedpod. *Adv Funct Mater*. 2017;27:1605446.
51. Wang S, Yang Z, Gong G, et al. Icephobicity of penguins spheniscus humboldti and an artificial replica of penguin feather with air-infused hierarchical rough structures. *J Phys Chem C*. 2016;120:15923-15929.
52. Barthlott W, Schimmel T, Wiersch S, et al. The salvinia paradox: superhydrophobic surfaces with hydrophilic pins for air retention under water. *Adv Mater*. 2010;22:2325-2328.
53. Parker AR, Lawrence CR. Water capture by a desert beetle. *Nature*. 2001;414:33-34.
54. Feng S, Zhu P, Zheng H, et al. Three-dimensional capillary ratchet-induced liquid directional steering. *Science*. 2021;373:1344-1348.
55. Wei J, Liang Y, Chen X, et al. Enhanced flexibility of the segmented honey bee tongue with hydrophobic tongue hairs. *ACS Appl Mater Interfaces*. 2022;14:12911-12919.
56. Liu M, Wang S, Wei Z, et al. Bioinspired design of a superoleophobic and low adhesive water/solid interface. *Adv Mater*. 2009;21:665-669.
57. Herminghaus S. Roughness-induced non-wetting. *Europhys Lett*. 2000;52:165.
58. Bormashenko E, Gendelman O, Whyman G. Superhydrophobicity of lotus leaves versus birds wings: different physical mechanisms leading to similar phenomena. *Langmuir*. 2012;28:14992-14997.
59. Yang C, Yang K, Li M, et al. The investigation of droplet directional self-transport ability on the slippery liquid-infused surface with anisotropic structure. *Prog Org Coat*. 2022;168:106857.
60. Yang Y, Li X, Zheng X, et al. 3d-printed biomimetic super-hydrophobic structure for microdroplet manipulation and oil/water separation. *Adv Mater*. 2018;30:1704912.
61. Sun Q, Wang D, Li Y, et al. Surface charge printing for programmed droplet transport. *Nat Mater*. 2019;18:936-941.
62. Dai R, Li G, Xiao L, et al. A droplet-driven micro-surfboard with dual gradients for programmable motion. *Chem Eng J*. 2022;446:136874.
63. Zhang X, Ben S, Zhao Z, et al. Lossless and directional transport of droplets on multi-bioinspired superwetting v-shape rails. *Adv Funct Mater*. 2023;33:2212217.
64. Wang F, Liu M, Liu C, et al. Light-induced charged slippery surfaces. *Sci Adv*. 2022;8:eabp9369.
65. Zhan H, Xia Y, Liu Y, et al. Sustainable droplet manipulation on ultrafast lubricant self-mediating photothermal slippery surfaces. *Adv Funct Mater*. 2023;33:2211317.
66. Barthlott W, Mail M, Bhushan B, Koch K. Plant surfaces: structures and functions for biomimetic innovations. *Nanomicro Lett*. 2017;9:23.
67. Sun Y, Guo Z. Recent advances of bioinspired functional materials with specific wettability: from nature and beyond nature. *Nanoscale Horiz*. 2019;4:52-76.
68. Irajizad P, Nazifi S, Ghasemi H. Icephobic surfaces: definition and figures of merit. *Adv Colloid Interface Sci*. 2019;269:203-218.
69. Irajizad P, Al-Bayati A, Eslami B, et al. Stress-localized durable icephobic surfaces. *Mater Horiz*. 2019;6:758-766.
70. Li X, Reinhoudt D, Crego-Calama M. What do we need for a superhydrophobic surface? A review on the recent progress in the preparation of superhydrophobic surfaces. *Chem Soc Rev*. 2007;36:1350-1368.
71. Ghasemlou M, Daver F, Ivanova EP, Adhikari B. Bio-inspired sustainable and durable superhydrophobic materials: from nature to market. *J Mater Chem A Mater*. 2019;7:16643-16670.
72. Arole VM, Munde SV. Fabrication of nanomaterials by top-down and bottom-up approaches-an overview. *J Mater Sci*. 2014;1:89-93.
73. Peng C, Chen Z, Tiwari MK. All-organic superhydrophobic coatings with mechanochemical robustness and liquid impalement resistance. *Nat Mater*. 2018;17:355-360.
74. Zhang H, Bu X, Li W, et al. A skin-inspired design integrating mechano–chemical–thermal robustness into superhydrophobic coatings. *Adv Mater*. 2022;34:2203792.
75. Ren H, Yang X, Wang Z, et al. Smart structures with embedded flexible sensors fabricated by fused deposition modeling-based multimaterial 3D printing. *Int J Smart Nano Mater*. 2022;13:447-464.
76. Moon CH, Yasmeen S, Park K, et al. Icephobic coating through a self-formed superhydrophobic surface using a polymer and microsized particles. *ACS Appl Mater Interfaces*. 2022;14:3334-3343.

77. Elzaabalawy A, Meguid SA. Development of novel icephobic surfaces using siloxane-modified epoxy nanocomposites. *Chem Eng J*. 2022;433:133637.
78. Zhu T, Cheng Y, Huang J, et al. A transparent superhydrophobic coating with mechanochemical robustness for anti-icing, photocatalysis and self-cleaning. *Chem Eng J*. 2020;399:125746.
79. Tian G, Zhang M, Zhao Y, et al. High corrosion protection performance of a novel nonfluorinated biomimetic superhydrophobic zn–fe coating with echinopsis multiplex-like structure. *ACS Appl Mater Interfaces*. 2019;11:38205-38217.
80. Tan Y, Hu B, Chu Z, Wu W. Bioinspired superhydrophobic papillae with tunable adhesive force and ultralarge liquid capacity for microdroplet manipulation. *Adv Funct Mater*. 2019;29:1900266.
81. Li W, Liu Y, Leng J. Harnessing wrinkling patterns using shape memory polymer microparticles. *ACS Appl Mater Interfaces*. 2021;13:23074-23080.
82. Chiera S, Koch VM, Bleyer G, et al. From sticky to slippery: self-functionalizing lubricants for in situ fabrication of liquid-infused surfaces. *ACS Appl Mater Interfaces*. 2022;14:16735-16745.
83. Zhang M, Chen P, Li J, Wang G. Water-repellent and corrosion resistance properties of epoxy-resin-based slippery liquid-infused porous surface. *Prog Org Coat*. 2022;172:107152.
84. Heydarian S, Jafari R, Momen G. Recent progress in the anti-icing performance of slippery liquid-infused surfaces. *Prog Org Coat*. 2021;151:106096.
85. Peppou-Chapman S, Hong JK, Waterhouse A, Neto C. Life and death of liquid-infused surfaces: a review on the choice, analysis and fate of the infused liquid layer. *Chem Soc Rev*. 2020;49:3688-3715.
86. Wong T, Kang SH, Tang SK, et al. Bioinspired self-repairing slippery surfaces with pressure-stable omniphobicity. *Nature*. 2011;477:443-447.
87. Quéré D. Non-sticking drops. *Rep Prog Phys*. 2005;68:2495.
88. Yan H, Zhang W, Cui Y, et al. Durable drag reduction and anti-corrosion for liquid flows inside lubricant-infused aluminum/copper capillaries. *Chem Eng Sci*. 2023;266:118275.
89. Zheng W, Teng L, Lai Y, et al. Magnetic responsive and flexible composite superhydrophobic photothermal film for passive anti-icing/active deicing. *Chem Eng J*. 2022;427:130922.
90. de Bruin KG, Bartolo D, Josserand C, et al. Maximum diameter of impacting liquid droplets. *Phys Rev Appl*. 2014;2:44018.
91. Lambley H, Schutzius TM, Poulikakos D. Superhydrophobic surfaces for extreme environmental conditions. *Proc Natl Acad Sci USA*. 2020;117:27188-27194.
92. Maitra T, Tiwari MK, Antonini C, et al. On the nanoengineering of superhydrophobic and impalement resistant surface textures below the freezing temperature. *Nano Lett*. 2014;14:172-182.
93. Srivastava T, Jena SK, Kondaraju S. Droplet impact and spreading on inclined surfaces. *Langmuir*. 2021;37:13737-13745.
94. Ding B, Wang H, Zhu X, et al. Water droplet impact on superhydrophobic surfaces with various inclinations and supercooling degrees. *Int J Heat Mass Transf*. 2019;138:844-851.
95. Wang Y, Xue J, Wang Q, et al. Verification of icephobic/anti-icing properties of a superhydrophobic surface. *ACS Appl Mater Interfaces*. 2013;5:3370-3381.
96. Liu Y, Moevius L, Xu X, et al. Pancake bouncing on superhydrophobic surfaces. *Nat Phys*. 2014;10:515-519.
97. Song D, Song B, Hu H, et al. Selectively splitting a droplet using superhydrophobic stripes on hydrophilic surfaces. *Phys Chem Phys*. 2015;17:13800-13803.
98. Gauthier A, Symon S, Clanet C, Quéré D. Water impacting on superhydrophobic macrotextures. *Nat Commun*. 2015;6:8001.
99. Song M, Liu Z, Ma Y, et al. Reducing the contact time using macro anisotropic superhydrophobic surfaces—effect of parallel wire spacing on the drop impact. *NPG Asia Mater*. 2017;9:e415.
100. Abolghasemibizaki M, Mohammadi R. Droplet impact on superhydrophobic surfaces fully decorated with cylindrical macrotextures. *J Colloid Interface Sci*. 2018;509:422-431.
101. Weisensee PB, Ma J, Shin YH, et al. Droplet impact on vibrating superhydrophobic surfaces. *Phys Rev Fluids*. 2017;2:103601.
102. Richard D, Clanet C, Quéré D. Contact time of a bouncing drop. *Nature*. 2002;417:811.
103. Wang Y, Wang Q, Ju L, Han DÉ, Xue Y. Numerical analysis on dynamics and thermodynamics of a supercooled water droplet considering the dynamic contact angle. *Phys Fluids*. 2021;33:102101.
104. Fang W, Zhu F, Shen F, et al. Freezing behaviors of impacting water droplets on cold inclined surfaces. *Appl Therm Eng*. 2023;219:119562.
105. Mishchenko L, Hatton B, Bahadur V, et al. Design of ice-free nanostructured surfaces based on repulsion of impacting water droplets. *ACS Nano*. 2010;4:7699-7707.
106. Chang S, Qi H, Zhou S, Yang Y. Experimental study on freezing characteristics of water droplets on cold surfaces. *Int J Heat Mass Transf*. 2022;194:123108.
107. Zhou X, Wang H, Wu J, et al. Bounce behaviors of double droplets simultaneously impact cold superhydrophobic surface. *Int J Heat Mass Transf*. 2023;208:124075.
108. Baek S, Moon HS, Kim W, et al. Effect of liquid droplet surface tension on impact dynamics over hierarchical nanostructure surfaces. *Nanoscale*. 2018;10:17842-17851.
109. Yeong YH, Sokhey J, Loth E. Ice adhesion on superhydrophobic coatings in an icing wind tunnel. In: Wohl CJ, Berry DH, eds. *Contamination Mitigating Polymeric Coatings for Extreme Environments*. Springer International Publishing; 2019:99-121.
110. Bird JC, Dhiman R, Kwon H, Varanasi KK. Reducing the contact time of a bouncing drop. *Nature*. 2013;503:385-388.
111. Shen Y, Tao J, Tao H, et al. Approaching the theoretical contact time of a bouncing droplet on the rational macrostructured superhydrophobic surfaces. *Appl Phys Lett*. 2015;107:111604.
112. Zhang H, Yi X, Du Y, et al. Dynamic behavior of water drops impacting on cylindrical superhydrophobic surfaces. *Phys Fluids*. 2019;31:32104.
113. Hu S, Cao X, Reddyhoff T, et al. Pneumatic programmable superrepellent surfaces. *Droplet*. 2022;1:48-55.
114. Schutzius TM, Jung S, Maitra T, et al. Physics of icing and rational design of surfaces with extraordinary icephobicity. *Langmuir*. 2015;31:4807-4821.
115. Tian Z, Wang L, Zhu D, et al. Passive anti-icing performances of the same superhydrophobic surfaces under static freezing, dynamic supercooled-droplet impinging, and icing wind tunnel tests. *ACS Appl Mater Interfaces*. 2023;15:6013-6024.
116. Golovin K, Dhyani A, Thouless MD, Tuteja A. Low–interfacial toughness materials for effective large-scale deicing. *Science*. 2019;364:371-375.
117. Liu Y, Li X, Jin J, et al. Anti-icing property of bio-inspired microstructure superhydrophobic surfaces and heat transfer model. *Appl Surf Sci*. 2017;400:498-505.
118. Zhang Y, Anim-Danso E, Bekele S, Dhinojwala A. Effect of surface energy on freezing temperature of water. *ACS Appl Mater Interfaces*. 2016;8:17583-17590.
119. Alizadeh A, Yamada M, Li R, et al. Dynamics of ice nucleation on water repellent surfaces. *Langmuir*. 2012;28:3180-3186.
120. Hou Y, Choy KL. Durable and robust pvdf-hfp/sio2/cnts nanocomposites for anti-icing application: water repellency, icing delay, and ice adhesion. *Prog Org Coat*. 2022;163:106637.
121. Wei J, Li B, Tian N, et al. Scalable robust superamphiphobic coatings enabled by self-similar structure, protective micro-skeleton, and adhesive for practical anti-icing of high-voltage transmission tower. *Adv Funct Mater*. 2022;32:2206014.

122. Guo P, Zheng Y, Wen M, et al. Icephobic/anti-icing properties of micro/nanostructured surfaces. *Adv Mater*. 2012;24:2642-2648.
123. Oberli L, Caruso D, Hall C, et al. Condensation and freezing of droplets on superhydrophobic surfaces. *Adv Colloid Interface Sci*. 2014;210:47-57.
124. Eberle P, Tiwari MK, Maitra T, Poulikakos D. Rational nanostructuring of surfaces for extraordinary icephobicity. *Nanoscale*. 2014;6:4874-4881.
125. Lambley H, Graeber G, Vogt R, et al. Freezing-induced wetting transitions on superhydrophobic surfaces. *Nat Phys*. 2023;19:649-655.
126. Emelyanenko KA, Emelyanenko AM, Boinovich LB. Water and ice adhesion to solid surfaces: common and specific, the impact of temperature and surface wettability. *Coatings (Basel)*. 2020;10:648.
127. Huré M, Olivier P, Garcia J. Effect of cassie-baxter versus wenzel states on ice adhesion: a fracture toughness approach. *Cold Reg Sci Technol*. 2022;194:103440.
128. Dhyani A, Choi W, Golovin K, Tuteja A. Surface design strategies for mitigating ice and snow accretion. *Matter*. 2022;5:1423-1454.
129. Golovin K, Kobaku SP, Lee DH, Diloreto ET, Mabry JM, Tuteja A. Designing durable icephobic surfaces. *Sci Adv*. 2016;2:e1501496.
130. Tong W, Xiong D, Wang N, et al. Mechanically robust superhydrophobic coating for aeronautical composite against ice accretion and ice adhesion. *Compos Part B: Engin*. 2019;176:107267.
131. Boinovich LB, Chulkova EV, Emelyanenko KA, et al. The mechanisms of anti-icing properties degradation for slippery liquid-infused porous surfaces under shear stresses. *J Colloid Interface Sci*. 2022;609:260-268.
132. Wang Y, Zhang J, Dodiuk H, et al. The effect of superhydrophobic coating composition on the topography and ice adhesion. *Cold Reg Sci Technol*. 2022;201:103623.
133. Li X, Wang G, Zhan B, et al. A novel icephobic strategy: the fabrication of biomimetic coupling micropatterns of superwetting surface. *Adv Mater Interfaces*. 2019;6:1900864.
134. Laroche A, Grasso MJ, Dolatabadi A, Bonaccurso E. Tensile and shear test methods for quantifying the ice adhesion strength to a surface. In: Mittal KL, Choi C-H, eds. *Ice Adhesion: Mechanism, Measurement and Mitigation*. Scrivener Publishing LLC; 2020:237-284.
135. Gao H, Yao H. Shape insensitive optimal adhesion of nanoscale fibrillar structures. *Proc Natl Acad Sci USA*. 2004;101:7851-7856.
136. Nosonovsky M, Hejazi V. Why superhydrophobic surfaces are not always icephobic. *ACS Nano*. 2012;6:8488-8491.
137. Kulinich SA, Farzaneh M. How wetting hysteresis influences ice adhesion strength on superhydrophobic surfaces. *Langmuir*. 2009;25:8854-8856.
138. Chen C, Tian Z, Luo X, et al. Micro–nano-nanowire triple structure-held PDMS superhydrophobic surfaces for robust ultra-long-term icephobic performance. *ACS Appl Mater Interfaces*. 2022;14:23973-23982.
139. Zhou W, Wu T, Du Y, et al. Efficient fabrication of desert beetle-inspired micro/nano-structures on polypropylene/graphene surface with hybrid wettability, chemical tolerance, and passive anti-icing for quantitative fog harvesting. *Chem Eng J*. 2023;453:139784.
140. Kulinich SA, Farhadi S, Nose K, Du XW. Superhydrophobic surfaces: are they really ice-repellent? *Langmuir*. 2011;27:25-29.
141. Boinovich LB, Emelyanenko KA, Emelyanenko AM. Superhydrophobic versus slips: temperature dependence and the stability of ice adhesion strength. *J Colloid Interface Sci*. 2022;606:556-566.
142. Jung S, Tiwari MK, Poulikakos D. Frost halos from supercooled water droplets. *Proc Natl Acad Sci USA*. 2012;109:16073-16078.
143. Eslami B, Irajizad P, Jafari P, et al. Stress-localized durable anti-biofouling surfaces. *Soft Matter*. 2019;15:6014-6026.
144. Nazifi S, Huang Z, Hakimian A, Ghasemi H. Fracture-controlled surfaces as extremely durable ice-shedding materials. *Mater Horiz*. 2022;9:2524-2532.
145. Kim J, Byun S, Lee J, Lee K. Frost growth behavior according to the cold surface inclination angle. *Int J Heat Mass Transf*. 2020;146:118841.
146. Meuler AJ, Mckinley GH, Cohen RE. Exploiting topographical texture to impart icephobicity. *ACS Nano*. 2010;4:7048-7052.
147. Farhadi S, Farzaneh M, Kulinich SA. Anti-icing performance of superhydrophobic surfaces. *Appl Surf Sci*. 2011;257:6264-6269.
148. Yan X, Zhang L, Sett S, et al. Droplet jumping: effects of droplet size, surface structure, pinning, and liquid properties. *ACS Nano*. 2019;13:1309-1323.
149. Wang L, Jiang G, Tian Z, et al. Superhydrophobic microstructures for better anti-icing performances: open-cell or closed-cell? *Mater Horiz*. 2023;10:209-220.
150. Cheng Y, Liu Y, Ye X, et al. Macrotextures-enabled self-propelling of large condensate droplets. *Chem Eng J*. 2021;405:126901.
151. Yao Y, Zhao TY, Machado C, et al. Frost-free zone on macrotextured surfaces. *Proc Natl Acad Sci USA*. 2020;117:6323-6329.
152. Sun K, Liu Z, Wei J, Wang T. Thermal performance of a vapor chamber with synergistic effects of droplet jumping and pillared-wick capillarity. *Int J Heat Mass Transf*. 2022;195:123167.
153. Chu F, Yan X, Miljkovic N. How superhydrophobic grooves drive single-droplet jumping. *Langmuir*. 2022;38:4452-4460.
154. Boreyko JB, Collier CP. Delayed frost growth on jumping-drop superhydrophobic surfaces. *ACS Nano*. 2013;7:1618-1627.
155. Vercillo V, Tonnicchia S, Romano JM, et al. Design rules for laser-treated icephobic metallic surfaces for aeronautic applications. *Adv Funct Mater*. 2020;30:1910268.
156. Bengaluru Subramanyam S, Kondrashov V, Rühe J, Varanasi KK. Low ice adhesion on nano-textured superhydrophobic surfaces under supersaturated conditions. *ACS Appl Mater Interfaces*. 2016;8:12583-12587.
157. Baheri FT, Poulikakos LD, Poulikakos D, Schutzius TM. Dropwise condensation freezing and frosting on bituminous surfaces at subzero temperatures. *Constr Build Mater*. 2021;298:123851.
158. Smith JD, Dhiman R, Anand S, et al. Droplet mobility on lubricant-impregnated surfaces. *Soft Matter*. 2013;9:1772-1780.
159. Graeber G, Dolder V, Schutzius TM, Poulikakos D. Cascade freezing of supercooled water droplet collectives. *ACS Nano*. 2018;12:11274-11281.
160. Yang S, Ying Y, Li W, et al. Efficient anti-frosting on discrete nanoclusters via spatiotemporal control of condensation frosting dynamics. *Chem Eng J*. 2023;465:142991.
161. Sadullah MS, Panter JR, Kusumaatmaja H. Factors controlling the pinning force of liquid droplets on liquid infused surfaces. *Soft Matter*. 2020;16:8114-8121.
162. Chen L, Huang S, Ras RH, Tian X. Omniphobic liquid-like surfaces. *Nat Rev Chem*. 2023;7:123-137.
163. Yang S, Li W, Song Y, et al. Hydrophilic slippery surface promotes efficient defrosting. *Langmuir*. 2021;37:11931-11938.
164. Lv FY, Zhang P, Orejon D, Askounis A, Shen B. Heat transfer performance of a lubricant-infused thermosyphon at various filling ratios. *Int J Heat Mass Transf*. 2017;115:725-736.
165. Anand S, Paxson AT, Dhiman R, et al. Enhanced condensation on lubricant-impregnated nanotextured surfaces. *ACS Nano*. 2012;6:10122-10129.
166. Hauer L, Wong WS, Donadei V, et al. How frost forms and grows on lubricated micro-and nanostructured surfaces. *ACS Nano*. 2021;15:4658-4668.
167. Sadullah MS, Launay G, Parle J, et al. Bidirectional motion of droplets on gradient liquid infused surfaces. *Commun Phys*. 2020;3:166.
168. Dai X, Sun N, Nielsen SO, et al. Hydrophilic directional slippery rough surfaces for water harvesting. *Sci Adv*. 2018;4:eaaq0919.
169. Lee C, Kim H, Nam Y. Drop impact dynamics on oil-infused nanostructured surfaces. *Langmuir*. 2014;30:8400-8407.

170. Muschi M, Brudieu B, Teisseire J, Sauret A. Drop impact dynamics on slippery liquid-infused porous surfaces: influence of oil thickness. *Soft Matter*. 2018;14:1100-1107.
171. Hao C, Li J, Liu Y, et al. Superhydrophobic-like tunable droplet bouncing on slippery liquid interfaces. *Nat Commun*. 2015;6:7986.
172. Zhang Y, Klittich MR, Gao M, Dhinojwala A. Delaying frost formation by controlling surface chemistry of carbon nanotube-coated steel surfaces. *ACS Appl Mater Interfaces*. 2017;9:6512-6519.
173. Zhang L, Gao C, Zhong L, et al. Robust photothermal superhydrophobic coatings with dual-size micro/nano structure enhance anti-/de-icing and chemical resistance properties. *Chem Eng J*. 2022;446:137461.
174. Zhang L, Guo Z, Sarma J, Dai X. Passive removal of highly wetting liquids and ice on quasi-liquid surfaces. *ACS Appl Mater Interfaces*. 2020;12:20084-20095.
175. Ma L, Zhang Z, Gao L, et al. An exploratory study on using slippery-liquid-infused-porous-surface (slips) for wind turbine icing mitigation. *Renew Energy*. 2020;162:2344-2360.
176. Yao X, Chen B, Morelle XP, Suo Z. Anti-icing propylene-glycol materials. *Extreme Mech Lett*. 2021;44:101225.
177. Vogel N, Belisle RA, Hatton B, et al. Transparency and damage tolerance of patternable omniphobic lubricated surfaces based on inverse colloidal monolayers. *Nat Commun*. 2013;4:2176.
178. Long Y, Yin X, Mu P, et al. Slippery liquid-infused porous surface (slips) with superior liquid repellency, anti-corrosion, anti-icing and intensified durability for protecting substrates. *Chem Eng J*. 2020;401:126137.
179. Chen J, Dou R, Cui D, et al. Robust prototypical anti-icing coatings with a self-lubricating liquid water layer between ice and substrate. *ACS Appl Mater Interfaces*. 2013;5:4026-4030.
180. Ozbay S, Yuceel C, Erbil HY. Improved icephobic properties on surfaces with a hydrophilic lubricating liquid. *ACS Appl Mater Interfaces*. 2015;7:22067-22077.
181. Gurumukhi Y, Chavan S, Sett S, et al. Dynamic defrosting on superhydrophobic and biphilic surfaces. *Matter*. 2020;3:1178-1195.
182. Boylan D, Monga D, Shan L, et al. Pushing the limit of beetle-inspired condensation on biphilic quasi-liquid surfaces. *Adv Funct Mater*. 2023;33:2211113.
183. Hou Y, Yu M, Shang Y, et al. Suppressing ice nucleation of supercooled condensate with biphilic topography. *Phys Rev Lett*. 2018;120:75902.
184. Ahmadi SF, Nath S, Iliff GJ, et al. Passive antifrosting surfaces using microscopic ice patterns. *ACS Appl Mater Interfaces*. 2018;10:32874-32884.
185. Ghosh A, Beaini S, Zhang BJ, et al. Enhancing dropwise condensation through bioinspired wettability patterning. *Langmuir*. 2014;30:13103-13115.
186. Jin Y, Wu C, Yang Y, et al. Inhibiting condensation freezing on patterned polyelectrolyte coatings. *ACS Nano*. 2020;14:5000-5007.
187. Wood MJ, Brock G, Kietzig AM. The penguin feather as inspiration for anti-icing surfaces. *Cold Reg Sci Technol*. 2023;213:103903.
188. Wang Z, Zhu Y, Liu X, et al. Temperature self-regulating electrothermal pseudo-slippery surface for anti-icing. *Chem Eng J*. 2021;422:130110.
189. Yang C, Li Z, Huang Y, et al. Continuous roll-to-roll production of carbon nanoparticles from candle soot. *Nano Lett*. 2021;21:3198-3204.
190. Matsubayashi T, Tenjimbayashi M, Manabe K, et al. Integrated anti-icing property of super-repellency and electrothermogenesis exhibited by pedot: pss/cyanoacrylate composite nanoparticles. *ACS Appl Mater Interfaces*. 2016;8:24212-24220.
191. Niu W, Chen GY, Xu H, et al. Highly transparent and self-healable solar thermal anti-/deicing surfaces: when ultrathin mxene multilayers marry a solid slippery self-cleaning coating. *Adv Mater*. 2022;34:2108232.
192. Wang L, Tian Z, Zhu D, et al. Environmentally adapted slippery-superhydrophobic switchable interfaces for anti-icing. *Appl Surf Sci*. 2023;626:157201.
193. Xie Z, Wang H, Geng Y, et al. Carbon-based photothermal superhydrophobic materials with hierarchical structure enhances the anti-icing and photothermal deicing properties. *ACS Appl Mater Interfaces*. 2021;13:48308-48321.
194. Sun H, Lin G, Jin H, et al. Experimental investigation of surface wettability induced anti-icing characteristics in an ice wind tunnel. *Renew Energy*. 2021;179:1179-1190.
195. Alasvand Zarasvand K, Pope C, Nazari S, et al. Durable metallic surfaces capable of passive and active de-icing. *Adv Eng Mater*. 2022;24:2200573.
196. Zhao Z, Zhu Y, Wang Z, et al. A biaxial stretchable, flexible electric heating composite film for de-icing. *Compos Part A: Appl Sci Manuf*. 2022;162:107124.
197. Lin C, Ma W, Zhang Y, et al. A highly transparent photo-electrothermal film with broadband selectivity for all-day anti-/de-icing. *Small*. 2023;19:2301723.
198. Liu X, Zhu Y, Wang Z, et al. A sandwich-structured intelligent anti-icing/de-icing film with ice-oriented power self-regulating performance. *J Mater Chem C Mater*. 2022;10:12213-12220.
199. Wan Y, Liu Y, Liu Y, et al. Flexible electrothermal hydrophobic self-lubricating tape for controllable anti-icing and de-icing. *ACS Appl Eng Mater*. 2023;1:669-678.
200. Azimi Dijvejin Z, Jain MC, Kozak R, et al. Smart low interfacial toughness coatings for on-demand de-icing without melting. *Nat Commun*. 2022;13:5119.
201. Ke C, Liu J, Liu Y, et al. Photothermal mof-based multifunctional coating with passive and active protection synergy. *ACS Appl Eng Mater*. 2023;1:1058-1068.
202. Zhang S, Zhang F, Zhang Z, et al. An electroless nickel plating fabric coated with photothermal chinese ink for powerful passive anti-icing/icephobic and fast active deicing. *Chem Eng J*. 2022;450:138328.
203. Timoshenko PE, Lerer A, Rochal SB. Terahertz frequency selective surfaces using heterostructures based on two-dimensional diffraction grating of single-walled carbon nanotubes. *Int J Smart Nano Mater*. 2023;14:21-35.
204. Zhang X, Sun X, Wang Y, Qin J. Tribological behavior of WC-Al_2O_3-graphene composite at different temperatures. *Int J Smart Nano Mater*. 2022;13:691-712.
205. Song L, Yang C, Zhang S, et al. Multifunctional photothermal phase-change superhydrophobic film with excellent light–thermal conversion and thermal-energy storage capability for anti-icing/de-icing applications. *Langmuir*. 2022;38:15245-15252.
206. Zhao Z, Chen H, Zhu Y, et al. A robust superhydrophobic anti-icing/de-icing composite coating with electrothermal and auxiliary photothermal performances. *Compos Sci Technol*. 2022;227:109578.
207. Jiang G, Chen L, Zhang S, Huang H. Superhydrophobic sic/cnts coatings with photothermal deicing and passive anti-icing properties. *ACS Appl Mater Interfaces*. 2018;10:36505-36511.
208. Xiang T, Chen X, Lv Z, et al. Stable photothermal solid slippery surface with enhanced anti-icing and de-icing properties. *Appl Surf Sci*. 2023;624:157178.
209. Guo M, Yu Q, Wang X, et al. Tailoring broad-band-absorbed thermoplasmonic 1d nanochains for smart windows with adaptive solar modulation. *ACS Appl Mater Interfaces*. 2021;13:5634-5644.
210. Wu S, Liang Z, Li Y, et al. Transparent, photothermal, and icephobic surfaces via layer-by-layer assembly. *Adv Sci (Weinh)*. 2022;9:2105986.
211. Xu D, Li Z, Li L, Wang J. Insights into the photothermal conversion of 2d mxene nanomaterials: synthesis, mechanism, and applications. *Adv Funct Mater*. 2020;30:2000712.

212. Zhao Y, Yan C, Hou T, et al. Multifunctional $Ti_3C_2T_x$ MXene-based composite coatings with superhydrophobic anti-icing and photothermal deicing properties. *ACS Appl Mater Interfaces*. 2022;14:26077-26087.
213. Curtis SM, Sielenkämper M, Arivanandhan G, et al. TiNiHf/SiO_2/Si shape memory film composites for bi-directional micro actuation. *Int J Smart Nano Mater*. 2022;13:293-314.
214. Shao Y, Du W, Fan Y, et al. Near-infrared light accurately controllable superhydrophobic surface from water sticking to repelling. *Chem Eng J*. 2022;427:131718.
215. Liu F, Wang Z, Pan Q. Intelligent icephobic surface toward self-deicing capability. *ACS Sustain Chem Eng*. 2019;8:792-799.
216. Sun X, Damle VG, Liu S, Rykaczewski K. Bioinspired stimuli-responsive and antifreeze-secreting anti-icing coatings. *Adv Mater Interfaces*. 2015;2:1400479.
217. Wang Y, Yao X, Wu S, et al. Bioinspired solid organogel materials with a regenerable sacrificial alkane surface layer. *Adv Mater*. 2017;29:1700865.
218. Zhao H, Sun Q, Deng X, Cui J. Earthworm-inspired rough polymer coatings with self-replenishing lubrication for adaptive friction-reduction and antifouling surfaces. *Adv Mater*. 2018;30:1802141.
219. Irajizad P, Hasnain M, Farokhnia N, et al. Magnetic slippery extreme icephobic surfaces. *Nat Commun*. 2016;7:13395.
220. Volkov AG, Foster JC, Markin VS. Signal transduction in mimosa pudica: biologically closed electrical circuits. *Plant, Cell & Environ*. 2010;33:816-827.
221. Wang H, Xiong X, Yang L, Cui J. Droplets in soft materials. *Droplet*. 2022;1:110-138.
222. Li Z, He X, Cheng J, et al. Hydrogel-elastomer-based stretchable strain sensor fabricated by a simple projection lithography method. *Int J Smart Nano Mater*. 2021;12:256-268.
223. Yao X, Ju J, Yang S, Wang J, Jiang L. Temperature-driven switching of water adhesion on organogel surface. *Adv Mater*. 2014;26:1895-1900.
224. Buddingh JV, Nakamura S, Liu G, Hozumi A. Thermo-responsive fluorinated organogels showing anti-fouling and long-lasting/repeatable icephobic properties. *Langmuir*. 2022;38:11362-11371.
225. Qian H, Liu B, Wu D, et al. Facile fabrication of slippery lubricant-infused porous surface with pressure responsive property for anti-icing application. *Colloids Surf A: Physicochem Eng Asp*. 2021;618:126457.
226. Shuang B, Zhou T, Han M, et al. Multifunctional magnetocontrollable superwettable-microcilia surface for directional droplet manipulation. *Adv Sci (Weinh)*. 2019;6:1900834.
227. Oh I, Keplinger C, Cui J, et al. Dynamically actuated liquid-infused poroelastic film with precise control over droplet dynamics. *Adv Funct Mater*. 2018;28:1802632.
228. Huang Y, Stogin BB, Sun N, et al. A switchable cross-species liquid repellent surface. *Adv Mater*. 2017;29:1604641.
229. Neuwirth M, Daly JW, Myers CW, Tice LW. Morphology of the granular secretory glands in skin of poison-dart frogs (dendrobatidae). *Tissue Cell*. 1979;11:755-771.
230. Erbil HY. Improvement of lubricant-infused surfaces for anti-icing applications. *Surf Innov*. 2016;4:214-217.
231. Hou Y, Weng D, Yu Y, et al. Near infrared light responsive surface with self-healing superhydrophobicity in surface chemistry and microstructure. *Appl Surf Sci*. 2022;598:153772.
232. Chen C, Chen Y, Yao H, et al. A dual-mode laser-textured ice-phobic slippery surface: low-voltage-powered switching transmissivity and wettability for thermal management. *Nanoscale*. 2022;14:4474-4483.
233. Gulfam R, Orejon D, Choi C, Zhang P. Phase-change slippery liquid-infused porous surfaces with thermo-responsive wetting and shedding states. *ACS Appl Mater Interfaces*. 2020;12:34306-34316.
234. Nekoonam N, Vera G, Goralczyk A, et al. Controllable wetting transitions on photoswitchable physical gels. *ACS Appl Mater Interfaces*. 2023;15:27234-27242.
235. Ze Q, Kuang X, Wu S, et al. Magnetic shape memory polymers with integrated multifunctional shape manipulation. *Adv Mater*. 2020;32:1906657.
236. Khalid MY, Arif ZU, Noroozi R, et al. 4D printing of shape memory polymer composites: a review on fabrication techniques, applications, and future perspectives. *J Manuf Process*. 2022;81:759-797.
237. Spiegel CA, Hackner M, Bothe VP, et al. 4D printing of shape memory polymers: from macro to micro. *Adv Funct Mater*. 2022;32:2110580.
238. Aubin CA, Gorissen B, Milana E, et al. Towards enduring autonomous robots via embodied energy. *Nature*. 2022;602:393.
239. Li X, Zhan B, Wang X, et al. Preparation of superhydrophobic shape memory composites with uniform wettability and morphing performance. *Compos Sci Technol*. 2024;247:110398.
240. Li X, Liu Y, Leng J. Large-scale fabrication of superhydrophobic shape memory composite films for efficient anti-icing and de-icing. *Sustain Mater Technol*. 2023;37:e00692.
241. Zhao Z, Li X, Wei D, et al. Design of superhydrophobic shape memory composites with kirigami structures and uniform wetting property. *Polymers (Basel)*. 2023;15:3738.
242. Ozbay S, Erbil HY. Ice accretion by spraying supercooled droplets is not dependent on wettability and surface free energy of substrates. *Colloids Surf A: Physicochem Eng Asp*. 2016;504:210-218.
243. Huang Z, Ghasemi H. Hydrophilic polymer-based anti-biofouling coatings: preparation, mechanism, and durability. *Adv Colloid Interface Sci*. 2020;284:102264.

SUPPORTING INFORMATION

Additional supporting information can be found online in the Supporting Information section at the end of this article.

How to cite this article: Li X, Liu Y, Zhang Z, Liu Y, Leng J. Icephobic materials and strategies: From bio-inspirations to smart systems. *Droplet*. 2024;3:e131. https://doi.org/10.1002/dro2.131